HELSINKI UNIVERSITY OF TECHNOLOGY
Faculty of Information and Natural Sciences

Eero Tölö

Quasiparticles in quantum Hall droplets

Master's thesis submitted in partial fulfillment of the requirements for the degree of Master of Science in Technology in the Degree Programme in Engineering Physics.

Espoo, August 13, 2008

Supervisor: Academy Professor Risto Nieminen
Instructor: Docent Ari Harju

TEKNILLINEN KORKEAKOULU
Informaatio- ja luonnontieteiden tiedekunta

DIPLOMITYÖN TIIVISTELMÄ

Tekijä: Eero Tölö
Koulutusohjelma: Teknillisen fysiikan koulutusohjelma
Pääaine: Fysiikka
Sivuaine: Matematiikka

Työn nimi:
Kvasihiukkaset kvantti-Hall-saarekkeilla

Title in English:
Quasiparticles in quantum Hall droplets

Professuurin koodi ja nimi: Tfy-105 Teoreettinen ja laskennallinen fysiikka
Työn valvoja: Akatemiaprofessori Risto Nieminen
Työn ohjaaja: Dosentti Ari Harju

Tiivistelmä:

Kvantti-Hall-ilmiössä kaksiulotteinen elektronikaasu magneettikentässä kondensoituu nestettä muistuttavaan makroskooppiseen kvanttimekaaniseen tilaan. Tälle tilalle on ominaista poikittaisjohtavuuden topologinen kvantittuminen kokonais- tai murtolukuisesti, joista jälkimmäisellä tapauksella on murtolukuisen varauksen ja eksoottisen statistiikan omaavat kvasihiukkasviritykset.

Matalilla energioilla kvantti-Hall-systeemin vapausasteet ovat puhtaasti topologisia, ja eri tilat jaetaan topologisen järjestyksen perusteella universaalisuusluokkiin. Kullakin universaalisuusluokalla on oma matalan energian efektiivinen kvanttikenttäteoriansa, joka sisältää tiedon kvasihiukkasten varauksista ja statistiikasta. Äärellisessä systeemissä kaksiulotteinen efektiivinen teoria redusoituu yksiulotteiseksi reunateoriaksi, jonka rakenne koodaa universaalisuusluokan topologisen järjestyksen.

Työssä tutkitaan laskennallisesti muutaman elektronin kvantti-Hall-saarekkeita ja niihin liittyviä kvasihiukkasia diagonalisoimalla Hamiltonin matriisi korkean magneettikentän approksimaatiossa. Elektronien välinen vuorovaikutus riippuu Landaun tasosta ja kokeellisen näytteen yksityiskohdista. Tuloksissa verrataan realistisilla vuorovaikutuksilla laskettuja tiloja eri universaalisuusluokkiin kuuluviin teoreettisiin malleihin tutkimalla tilavektorien sisätuloa, aaltofunktioiden vaiherakennetta sekä kvasihiukkas- ja reunavirityksiä.

Sivumäärä: 81 Avainsanat: Murtolukuinen kvantti-Hall-ilmiö, kvasihiukkanen, kvanttipiste, eksakti diagonalisointi

Täytetään tiedekunnassa
Hyväksytty: Kirjasto:

HELSINKI UNIVERSITY OF TECHNOLOGY
Faculty of Information and Natural Sciences

ABSTRACT OF MASTER'S THESIS

Author: Eero Tölö
Degree Programme: Degree Programme in Engineering Physics
Major subject: Physics
Minor subject: Mathematics

Title:
Quasiparticles in quantum Hall droplets

Title in Finnish:
Kvasihiukkaset kvantti-Hall-saarekkeilla

Chair: Tfy-105 Theoretical and computational physics
Supervisor: Academy Professor Risto Nieminen
Instructor: Docent Ari Harju

Abstract:

In the quantum Hall effect, a planar electron gas exposed to a perpendicular magnetic field condenses into a macroscopic quantum mechanical liquid characterized by a topological integer or fractional quantization of the transverse conductance. For the fractionally quantized liquid, the low-energy elementary excitations carry fractional charge and obey fractional statistics.

At low energies, the degrees of freedom in the quantum Hall states are purely topological. The states are classified into universality classes according to their topological order, and for each universality class, there is a low-energy effective quantum field theory, which determines the properties of the associated quasiparticles. In a finite system with a boundary, the two-dimensional effective theory reduces into a one-dimensional edge theory, characteristic of each universality class.

The thesis investigates few-electron quantum Hall droplets and the associated quasiparticles by means of numerical exact diagonalization of the Hamiltonian matrix in a high magnetic field approximation, which constitutes a Landau level projection. The inter-electron interaction depends on the Landau level and the details of the experimental sample. In the results, we compare the states obtained with realistic effective interactions to the theoretical models concerning the universality classes of the Laughlin states and the Pfaffian state, by studying overlaps of the state vectors, phase structure of the wave functions, as well as the quasiparticle and edge excitations.

Number of pages: 81
Keywords: Fractional quantum Hall effect, quasiparticle, quantum dot, exact diagonalization

Faculty fills
Approved:
Library code:

Acknowledgements

This thesis was done at the Quantum many-body physics group in Helsinki University of Technology, and was supported by the Helsinki Institute of Physics. I wish to thank my instructor Ari Harju who came up with the subject and was helpful through the course of the work. I also thank Christian Webb, Jaakko Nissinen, and Jani Särkkä for interaction (we worked in the same room), and two of them for some interaction matrix element codes that were used in the work.

Espoo, August 13, 2008

Eero Tölö

Contents

Chapter 1

Introduction

This thesis explores the quasiparticle excitations in certain ground-states of the fractionally quantized Hall effect. These are anyons that interestingly carry a fraction of the elementary charge and unusual braiding statistics. Moreover, the recently discovered promising possibility of utilizing the plausibly non-Abelian anyons of the so-called $\frac{5}{2}$-state in a fault-tolerant topogical quantum computer offers a concrete and remarkable engineering application.

On the numerical side, we apply the exact diagonalization method, which is essentially nonperturbative but restricted to only small particle numbers. Therefore, the numerical results apply to few-electron droplets that can be realized in a quantum dot, or can be considered as an approximation for what occurs in the thermodynamic limit.

The remainder of this introduction reviews the basics of Hall effects, anyons, and quantum dots. Chapter 2 developes the theoretical understanding of the fractional quantum Hall effect in terms of low-energy effective theories. Chapter 3 presents the numerical methods for the study of few-electron quantum Hall droplets, while Chapter 4 contains selected numerical results.

1.1 Quantum Hall effects

Consider a situation where electrons are constricted to move in the x-y plane and exposed to a magnetic field perpendicular to the plane. Such a system can well be realized, for example, in a modulation-doped GaAs/AlGaAs semiconductor heterostructure interface [1]. The conduction-band energy in AlGaAs is higher than in GaAs, so that the electrons from Si donors placed in the AlGaAs, a distance away from the interface, transfer to the lower energy conduction-band of GaAs. Due to the distance, the scattering of electrons from the ionized dopants is reduced and the electrons are free to move in the plane. The motion in the z-direction is effectively damped by the bending of the conduction bands, and thus the electron gas can be considered two-dimensional to a good approximation.

A key observable in the quantum Hall experiment is the transverse Hall conductance. In two dimensions, conductance is scale invariant and equivalent with conductivity. This is essential for the universality of the result, since the size of the sample cannot usually be measured accurately enough. In an ideal system with no preferred frame of reference, the Hall conductivity is then easily obtained by a Lorentz transformation. If the electromagnetic fields in the frame of static electrons are $\mathbf{E}' = \mathbf{0}$ and $\mathbf{B}' = B\mathbf{e}_z$, then in the inertial frame moving at velocity $-\mathbf{v}$, the current density is $\mathbf{j} = -ne\mathbf{v}$ and the fields are $\mathbf{E} = -\mathbf{v} \times \mathbf{B}$ and $\mathbf{B} = \mathbf{B}'$ to lowest order in $\frac{v}{c}$. Hence,

$$\mathbf{E} = \frac{\mathbf{j} \times \mathbf{B}}{ne} = \frac{B}{ne} \begin{pmatrix} & 1 \\ -1 & \end{pmatrix} \mathbf{j} \equiv \underline{\rho}\, \mathbf{j}\,, \tag{1.1.1}$$

where $\underline{\rho}$ is the resistivity tensor. The conductivity tensor is the inverse

$$\underline{\sigma} = \underline{\rho}^{-1} = \frac{ne}{B} \begin{pmatrix} & -1 \\ 1 & \end{pmatrix}. \tag{1.1.2}$$

The above derived result that $\sigma_H \propto B^{-1}$ holds both in classical and quantum theory as it essentially relies only on the Lorentz covariance. However, in an actual experiment, at temperature of few Kelvins or less, the measured Hall conductance is quantized with great accuracy to plateaus proportional to a universal constant

$$\sigma_H = \frac{\nu e^2}{h}. \tag{1.1.3}$$

The longitudinal resistance almost vanishes at the plateaus, indicating nearly dissipationless current flow. The so-called filling factor, or filling fraction, ν depends on the electron

density and the strength of the external magnetic field, and it is observed to have around dozens of specific values. There is a distinction between integer [2] and fractional [3] quantum Hall effect depending on whether ν is an integer or a fraction. The fractional ν are observed only in the purest samples. While the integer plateaus are understood in terms of disorder induced localization (Anderson localization) where interaction of electrons can be neglected, the fractions turn out to be manifestation of strongly correlated electrons condensing to new kind of ground-states (though the localization is still needed for the plateaus), much like the condensation of electrons to the superconducting state in the conventional superconductors. The two Hall effects are, nonetheless, intimately related as is seen below.

1.1.1 Landau levels and the integer effect

To make progress in understanding the quantum Hall effects, consider a single free electron on a plane exposed to a perpendicular uniform magnetic field. We next solve the eigenfunctions, which are also later used as the basis in the numerical diagonalization of the interacting system. The Hamiltonian is written in the symmetric gauge $\mathbf{A} = (y, -x)\frac{B}{2}$ as

$$H = \frac{1}{2m}\left(\frac{\hbar}{i}\nabla + e\mathbf{A}\right)^2 = -\frac{\hbar^2}{2m}\nabla^2 + \frac{(eBr)^2}{8m} - \frac{eBM}{2m}\,. \tag{1.1.4}$$

Here $M = i\hbar(y\partial_x - x\partial_y)$ is the operator for the z-component of the angular momentum. Since we are working in two-dimensions, the angular momentum is henceforth the z-component of the angular momentum. It is convenient to use the complex co-ordinate $z = \frac{1}{2}(x + iy)$ and $\partial = \partial_z$, and define $\omega_c = \frac{eB}{m}$ and $l_c = \sqrt{\frac{\hbar}{m\omega_c}}$. These give then $M = \hbar(z\partial - \bar{z}\bar{\partial})$ and

$$H = -\frac{\hbar^2}{2m}\partial\bar{\partial} + \frac{1}{2}m\omega_c^2 z\bar{z} - \frac{\omega_c}{2}M\,. \tag{1.1.5}$$

The spectrum is easily solved by introducing the lowering operators

$$a = -\frac{i}{\sqrt{2}}\left(\frac{z}{l_c} + l_c\bar{\partial}\right) \quad \text{and} \quad b = \frac{1}{\sqrt{2}}\left(\frac{\bar{z}}{l_c} + l_c\partial\right)\,, \tag{1.1.6}$$

which along with the adjoint operators obey commutation relations $[a, a^\dagger] = [b, b^\dagger] = 1$ and $[a, b] = [a, b^\dagger] = 0$. The Hamiltonian is rewritten as

$$H = (a^\dagger a + \frac{1}{2})\hbar\omega_c\,. \tag{1.1.7}$$

As in the usual treatment of a harmonic oscillator, the eigenvalues are $(n+\frac{1}{2})\hbar\omega_c$ with non-negative integer n and the lowest energy states satisfy $a\Psi_0 = (\frac{z}{l_c}+l_c\bar{\partial})\Psi_0 = 0$. From now on, we work in the units where $l_c = 1$ and $\hbar\omega_c = 1$. The ground-states are then of the form $\Psi_0 = f(z)\exp(-z\bar{z})$, where $f(z)$ is a properly normalized analytic function. Since $[H, M] = 0$, it is convenient to diagonalize both energy and angular momentum simultaneously. Rewriting M as $M = b^\dagger b - a^\dagger a$ leads us to condition $b\Psi_0 = (\bar{z}+\partial)\Psi_0 = 0$ for the lowest angular momentum energy eigenstate. This is equivalent to $\partial f(z) = 0$, so that after proper normalization $f(z) = \frac{1}{\sqrt{2\pi}}$. We can define $|0\rangle = |0,0\rangle$ by $a|0\rangle = b|0\rangle = 0$. Then, a complete basis of eigenstates of H is given by the raising operators as

$$|n,l\rangle = |n, m-n\rangle = \frac{1}{\sqrt{n!m!}}(a^\dagger)^n(b^\dagger)^m|0\rangle\,, \tag{1.1.8}$$

with $H|n,l\rangle = (n+\frac{1}{2})|n,l\rangle$, $M|n,l\rangle = l|n,l\rangle$, and integer $l \geq -n$. In the co-ordinate representation, after rescaling $z \mapsto \frac{z}{2}$, so that $z = x+iy$, the wave function reads [4]

$$\psi_{nl}(z) = \sqrt{\frac{n!}{2^{l+1}\pi(n+l)!}}z^l L_n^l\left(\frac{z\bar{z}}{2l_c^2}\right)\exp\left(-\frac{z\bar{z}}{4l_c^2}\right), \tag{1.1.9}$$

where L_n^l is a generalized Laguerre polynomial. The first three polynomials relevant to this work are

$$\begin{aligned} L_0^l(x) =& 1\,, \\ L_1^l(x) =& -x+l+1\,, \\ L_2^l(x) =& \frac{x^2}{2} - (l+2)x + \frac{(l+2)(l+1)}{2}\,. \end{aligned} \tag{1.1.10}$$

The non-negative integer n labels the Landau levels each separated by energy $\hbar\omega_c$, which is proportional to the magnetic field. Asymptotically, the probability density $\psi_{nl}\bar{\psi}_{nl} \propto r^{2(n+l)}\exp(-\frac{r^2}{2l^2})$ and has a sharp peak at $r_n = \sqrt{2(n+l)}l_c$. In free space each Landau level is infinite-fold degenerate, but in an actual sample the Landau levels bend at the edge of the system as in Figure 1.1a. In the macroscopic limit, relating $r_{n+l_{\max}}$ with the sample size gives degeneracy $d = \frac{A}{2\pi l_c^2} \propto B$ in a sample of area A, for each Landau level.

The integer quantum Hall effect can now be understood in terms of filling of subsequent Landau levels in the presence of weak disorder. Combination of the ideal value and the experimental result for σ_H (Equations (1.1.2) and (1.1.3)) gives

$$\nu = \frac{N}{\Phi/\Phi_0}\,, \tag{1.1.11}$$

where N is the number of electrons in a sample threaded by a magnetic flux $\Phi = AB$. The flux unit $\Phi_0 = \frac{h}{e} = 2\pi l_c^2 B$. According to the degeneracy calculated above, $\Phi/\Phi_0 = d$. Hence, for n filled Landau levels $\nu = n$, which also explains why ν is called the filling fraction. When the spin is incorporated, $\nu = 2$ corresponds to the lowest Landau levels of both spin types fully occupied. This leads us to think that the integer values of Hall conductance are caused by electrons occupying full Landau levels. The excess electrons that do not fit to the last filled Landau level are localized at impurities of the sample material and hence do not contribute to the Hall current. To be specific, in the presence of disorder the Landau levels broaden in energy, and between these Landau bands emerge localized states as shown in Figure 1.1a. When the Fermi energy lies in the mobility gap (i.e., between two shaded areas in the figure), the Hall conductance is quantized in accordance with the number of filled Landau levels. The bending of the Landau levels near the edge gives rise to states at the Fermi level (Figure 1.1b), which, being gapless, are more likely carriers of longitudinal currents than the bulk states that have a large excitation gap. There exists also a powerful gauge argument for the conductivity, generalization of which to fractional conductivities is outlined later in this section.

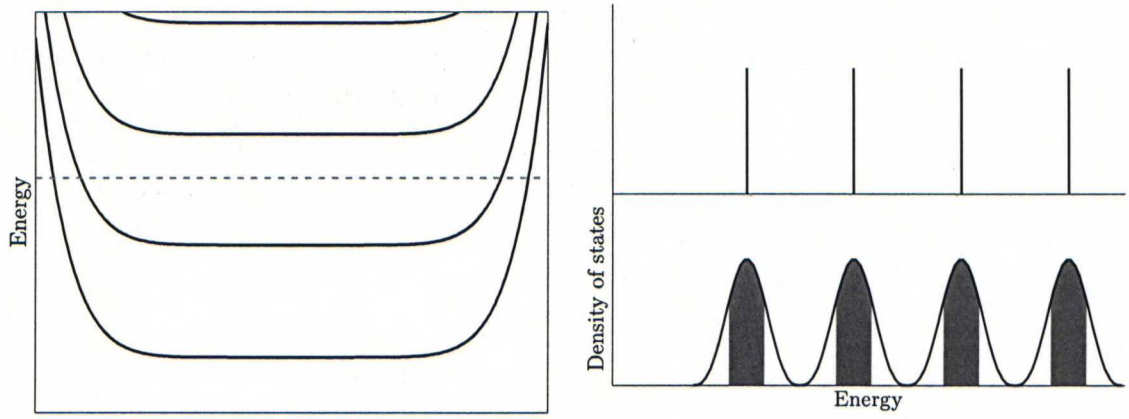

Figure 1.1: (a) Bending of the Landau levels at the edge of the system. (b) Density of states in an ideal and disordered system. In lower curves, the shading marks the position of extended states.

1.1.2 The fractional effect and composite-fermions

The fractional quantum Hall effect is far less transparent than the integer counterpart. While most of the observed fractions ν are now derived in terms of integer Hall effect of composite-fermions composed of flux and electrons, there still exists observed fractions such as $\frac{5}{2}$ and possibly $\frac{12}{5}$, whose interpretation is still unknown and the existing theories rely ultimately on guesswork supported by numerical studies with few electrons. For a partially filled Landau level, say $\nu = \frac{1}{3}$, the degeneracy of the ground-state of the non-interacting system is colossal (actually $\binom{d}{\nu d}$). Within such environment, a macroscopic organization of the electrons as to minimize the energy due to impurities and Coulomb interaction takes place and gives rise to a unique ground-state. These states manifest themselves in the fractionalized Hall conductance.

An efficient way to reduce the Coulomb energy between electrons is the attachment of flux to the position of electrons. Recall that the Aharonov-Bohm phase [5] for an electron moving around a closed path enclosing flux Φ is $\exp(\frac{2\pi i}{\Phi_0}\oint \mathrm{d}\mathbf{l}\cdot\mathbf{A}) = \exp(\frac{2\pi i\Phi}{\Phi_0})$. If we attach a fictitious delta function flux to the position of each electron $\Phi(z) = \sum_i \Phi_0 m\delta(z - z_i)$, and consider the electron-flux composites as the fundamental particles, then the phase factor acquired when two free composite-particles are interchanged ($\frac{1}{2}$ winding) is $e^{\pi i m}$. Such flux attachment procedure constitutes a statistical transmutation. If m is even integer, the phase is minus one and the composites are fermions. For odd integer m the composites are bosons, and for general real m, the composites are anyons discussed in detail in the later section. The above discussion suggests that multiplying the wave function of composite-fermions by a factor proportional to $\prod_{i<j}(z_i - z_j)^{2m}$ with positive integer m turns it into the corresponding wave function for electrons, since it then satisfies the antisymmetry requirement and contains the additional exhange phase due to the flux tubes. Imagine that the composite-fermions have the Slater determinant wave function of the filled lowest Landau level (we constantly drop the irrelevant normalization constants in the wave functions)

$$\Psi_{\nu=1}(z_1, z_2, \ldots, z_N) = \prod_{i<j}(z_i - z_j)e^{-\sum_i z_i\bar{z}_i/4l_c^2}, \tag{1.1.12}$$

and multiply it by the conversion factor. The result is

$$\Psi(z_1, z_2, \ldots, z_N) = \prod_{i<j}(z_i - z_j)^{2m+1}e^{-\sum_i z_i\bar{z}_i/4l_c^2}, \tag{1.1.13}$$

which seems like a perfectly good candidate for a ground-state wave function on the lowest Landau level, as the Jastrow factor is an analytic polynomial, and the electrons tend to avoid each other strongly. The maximal power of z_i in Ψ_ν is $(2m+1)(N-1)$ so the area is $A = (2m+1)(N-1)2\pi l_c^2$, which in turn yields filling fraction

$$\nu = \frac{N}{d} = \frac{N}{\frac{A}{2\pi l_c^2}} \xrightarrow{N\to\infty} \frac{1}{2m+1} . \tag{1.1.14}$$

The Ψ in Equation (1.1.13) is the celebrated Laughlin wave function [6] for the primary filling fractions $\frac{1}{2m+1}$ on the lowest Landau level. Exact diagonalization studies with few electrons in different geometries show exceptionally strong numerical evidence in favor of the Laughlin wave function. Later in this work, we examine the low-energy excitations of the Laughlin states and their counterparts in a quantum dot theoretically and numerically.

Essential in the previous reasoning was the starting point of a filled Landau level occupied by composite-fermions. Following Jain [7], we think about the partition function of the interacting system expressed as a path-integral over closed paths in the configuration-space. The contributions come from the Aharonov-Bohm phase and the statistical phase of fermions. The stability of filled Landau levels, and hence the integer quantum Hall effect of electrons, presumably takes place due to complicated correlations in these phase factors, and attachment of even number of flux tubes to electrons should maintain these correlations, since the composite-particles still remain fermions. Although a bit vague in nature, the argument explains most of the observed odd-denominator fractions and predicts the order of stability of the fractions in remarkable, though not perfect, agreement with the experiments. Let the Landau levels up to $\pm p$ to be occupied by composite-fermions composed of electron and $2m$ flux quanta ($\pm$ corresponds to the two possible directions of the magnetic field). The number of flux quanta per electron is $2m \pm p^{-1}$, so that the filling fraction is $\nu = \frac{N}{\Phi/\Phi_0} = \frac{p}{2mp\pm 1}$. This implies the stability of fractions

$$\nu = n + \frac{p}{2mp \pm 1} \quad \text{and} \quad \nu = n + 1 - \frac{p}{2mp \pm 1} , \tag{1.1.15}$$

where the latter follow from the electron-hole symmetry. More fractions can be obtained as daughter states by various hierarchy schemes [8, 9]. We still need to show that the filling fractions lead to the right conductances.

The conductance can be derived by utilizing the universality of the effect [10, 11]. In particular, the conductance should be insensitive to continuous deformation of the sample geometry. In what follows, we outline a variation of this argument. The assumptions

are the same as earlier summarized in Figure 1.1a. The rectangular Hall bar can be deformed to an annulus where the longitudinal driving voltage is replaced by a magnetic flux threading the hole of the annulus, as shown in Figure 1.2.

In the limit of the radius of the hole going to zero, the lowest Landau level states read

$$\psi(z) = z^{l+\Phi/\Phi_0} \exp\left(-\frac{z\bar{z}}{4l_c^2}\right) , \tag{1.1.16}$$

with integer l such that $l+\Phi/\Phi_0 \geq 0$. Adiabatic increment of the flux from 0 to Φ_0 affects spectral flow in which $z^l \mapsto z^{l+1}$ †, and a similar statement holds for all the other Landau levels. For a compactly filled Landau level, the net effect is to transfer one electron from the center to the edge of the system. The change in the energy of the sample is $-neV$, where V is the voltage difference between the center and the edge, and n is the number of filled Landau levels. The energy is equal to the work done in the flux change $-I\Phi_0$. Thus,

$$\sigma = \frac{I}{V} = \frac{ne}{\Phi_0} = \frac{ne^2}{h} , \tag{1.1.17}$$

which explains the conductance of the integer effect. For $\pm p$ filled composite-fermion Landau levels, $2mp$ additional flux quanta are needed as each electron now carries flux $2m\Phi_0$. The work done to transport p electrons is equal to $-I(2m \pm 1)\Phi_0$, so that

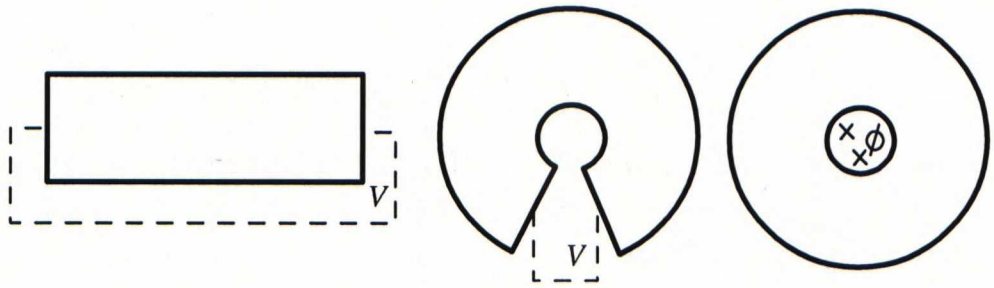

Figure 1.2: Deformation of voltage driven Hall bar to flux penetrated annulus.

† We have slightly simplified the picture for sake of clarity. In fact, the net effect of adding a flux quantum amounts to the singular gauge transformation $\psi_{0l} \mapsto e^{i\theta}\psi_{0l} = \sum_{m=0}^{\infty} \alpha_m^l \psi_{m,l+1}$, where ψ_{nl} are as in Equation (1.1.9), $z = re^{i\theta}$, and the expansion coefficients are evaluated with the aid of orthogonality relation of the generalized Laguerre polynomials:
$\alpha_m^l = \sqrt{\frac{m!}{l!(m+l+1)!}} \int_0^\infty \mathrm{d}\xi \xi^{l+\frac{1}{2}} L_m^{l+1}(\xi) e^{-\xi}$.
In a good approximation, the transformed wave function is projected to the lowest Landau level $\alpha_m^l = \delta_{m0}$, and the approximation gets better as l increases.

$$\sigma = \frac{I}{V} = \frac{ne}{\Phi_0} = \frac{(2mp \pm 1)}{p}\frac{e^2}{h}, \tag{1.1.18}$$

as it should. As in the integer quantum Hall effect, sample impurities and inhomogeneities create localized states, which produce the conductance plateaus as long as the Fermi energy is in the mobility gap. As the culmination of the gauge argument, with some effort, the Hall conductance can be identified as a topological invariant, the first Chern class of the $U(1)$ principal bundle over the torus $T \times T$ [1, 12, 13].

1.1.3 Quasiparticles in the FQHE

A famous hallmark of the fractional quantum Hall effect are the recently observed [14, 15] quasiparticles, which carry fractional charge and obey fractional statistics. In context of the above presented gauge argument, $2m \pm 1$ flux quanta was needed to transfer a composite-fermion from the center to the edge leaving behind a hole of charge e. This suggests that threading a single flux quantum through the origin amounts to creation of a quasihole of charge $\frac{e}{2m\pm1}$ at the center. In the following calculation, we consider the situation with $p = 1$. In the lowest Landau level projected wave function, the flux-threading amounts to multiplication by the factor $\prod_i z_i$ as the angular momentum of each single-particle state is increased by one. For a quasihole at position η the wave function becomes

$$\Psi_\nu^{\mathrm{QH}}(z_1, z_2, \ldots, z_N) = \left[\prod_{i=1}^{N}(z_i - \eta)\right] \Psi_\nu(z_1, z_2, \ldots, z_N)\,. \tag{1.1.19}$$

The charge of the quasihole q is obtained by comparing the Berry phase (see Section 3.4) associated with the adiabatic transport of the quasihole around a closed, say anticlockwise, path C enclosing flux Φ to the corresponding Aharonov-Bohm phase [16]

$$\gamma_{\mathrm{AB}} = -\frac{2\pi\frac{q}{e}}{\Phi_0}\oint_C \mathrm{d}\mathbf{l}\cdot\mathbf{A} = -\frac{2\pi\Phi}{\Phi_0}\frac{q}{e}\,. \tag{1.1.20}$$

Denoting $\Psi = \Psi_\nu^{\mathrm{QH}}$, the Berry phase is

$$\begin{aligned}\gamma &= i\oint_C \mathrm{d}t\langle\Psi(\eta(t))|\frac{d}{dt}|\Psi(\eta(t))\rangle = i\oint_C \mathrm{d}\eta\langle\Psi(\eta)|\partial_\eta|\Psi(\eta)\rangle \\ &= i\oint_C \mathrm{d}\eta\langle\Psi(\eta)|\left[\partial_\eta\sum_i \ln(z_i - \eta)\right]|\Psi(\eta)\rangle\end{aligned}$$

$$
\begin{aligned}
&= i \oint_C \mathrm{d}\eta \int \mathrm{d}x\mathrm{d}y \langle \Psi(\eta)| \left[\sum_i (\delta(z - z_i)) \partial_\eta \ln(z - \eta) \right] |\Psi(\eta)\rangle \\
&= i \oint_C \mathrm{d}\eta \int \mathrm{d}x\mathrm{d}y \rho(z) \partial_\eta \ln(z - \eta) \, .
\end{aligned}
\tag{1.1.21}
$$

The density $\rho = \langle \Psi | \sum_i \delta(z - z_i) | \Psi \rangle$ consists of the uniform density in the absence of the quasihole ρ_0 and a small perturbation $\delta\rho$ due to the quasihole, which divides the Berry phase similarly into $\gamma = \gamma_0 + \delta\gamma$. To get the γ_0-contribution, note that the pole $\oint_C \mathrm{d}w \partial_w \ln(z - w)$ gives $2\pi i$ if C encloses z and 0 otherwise. The wave function picks up a phase factor that counts the mean number of electrons enclosed by the path

$$
\gamma_0 = -2\pi \int_{<C} \mathrm{d}x\mathrm{d}y \rho_0(z) = -2\pi N_< = -\frac{2\pi\nu\Phi}{\Phi_0} \, . \tag{1.1.22}
$$

The correction term $\delta\gamma$ due to finite size of the quasihole is $\mathcal{O}(\frac{l_c^2}{A})$ when loop encloses area A and should be neglected. Comparison with Equation (1.1.20) gives

$$
q = \nu e \, , \tag{1.1.23}
$$

so the charge is a fraction of the elementary charge. The fractional charge clearly implies that quasiparticles have also fractional statistics. The wave function for two quasiholes is

$$
\Psi_\nu^{\mathrm{QH}}(z_1, z_2, \ldots, z_N) = \left[\prod_{i=1}^{N} (z_i - \eta_1)(z_i - \eta_2) \right] \Psi_\nu(z_1, z_2, \ldots, z_N) \, . \tag{1.1.24}
$$

As above, let η_1 go around a closed path. If the quasihole at η_2 is wholly outside the path, γ is as above. If η_2 is well inside the path, $N_<$ is reduced by ν, so that due to vorticity, additional statistical phase factor $\Delta\gamma = 2\pi\nu$ emerges. For integer $\nu = 1$, the quasiholes are fermionic but in general they are anyons, discussed more thoroughly in the next section. The observation of the fractional charge ten years ago lead to the Nobel prize for the early FQHE pioneers Tsui, Stormer and Laughlin. The fractional statistics has been observed only recently in interferometer experiments [14, 15].

To create a quasielectron, or antivortex, we thread the flux to the opposite direction. In the approximation analogous to that in the previous footnote, the polynomial factor of the single particle states evolves $z^l \mapsto z^{l-1}$, except for the case $l = 0$, which maps completely to the higher Landau levels and is projected out. The mapping is implemented by the factor $\prod_i \partial_i$ acting only on the polynomial part of the wave function, or by the factor $\prod_i (\partial_i - \frac{\bar{\eta}}{4l_c^2})$ for a quasielectron positioned at η. Kjønsberg, Leinaas, and Myrheim [17,

18] have studied the quasiparticle charge and statistics in system of 20 to 200 electrons at $\nu = \frac{1}{3}$ by computing the Berry phase for quasiparticle traversing around a circular loop enclosing zero to one other quasiparticles using Monte Carlo method with the above derived Laughlin's quasiparticle wave functions. They find quite accurately the charge $\pm\frac{e}{3}$ corresponding to quasihole and quasielectrons when the quasiparticles are not too close to the edge of the droplet. They also obtain the correct fractional statistics for two quasiholes that are well separated. This is not the case for the quasielectrons, unless they use the trial wave function that follows from Jain's composite-fermion theory,

$$\begin{aligned}\Psi^{\mathrm{QE}}_{\frac{1}{2m+1}} &= e^{-\sum_i z_i\bar{z}_i/4l_c^2}\begin{vmatrix} \bar{z}_1 & \bar{z}_2 & \cdots & \bar{z}_N \\ 1 & 1 & \cdots & 1 \\ z_1 & z_2 & \cdots & z_N \\ \vdots & \vdots & \cdots & \vdots \\ z_1^{N-2} & z_2^{N-2} & \cdots & z_N^{N-2} \end{vmatrix}\prod_{i<j}(z_i - z_j)^{2m} \\ &= e^{-\sum_i z_i\bar{z}_i/4l_c^2}\sum_{i=1}^{N}\left(\frac{\bar{z}_i}{\prod_{j\neq i}(z_i - z_j)}\right)\prod_{i<j}(z_i - z_j)^{2m+1}\,.\end{aligned} \tag{1.1.25}$$

As seen in Equation (1.1.22), the moving quasiparticles develop Aharonov-Bohm-type phases as if they saw electron density as flux density. The vortices behave as the lowest Landau level states of charged particles in a magnetic field. This gives rise to a duality of the model in which the quasiparticles themselves can Bose condense and is the basis of the Haldane-Halperin hierarchy scheme [19, 20], which can be used to derive, starting from a primary filling fraction $\frac{1}{2m+1}$, a hierarchy of descendant fractions. The hierarchy scheme, however, suffers from quite a few annoyances and has lately lost much of its credibility. For instance, to construct the fraction $\nu = \frac{2}{5}$, one needs $\frac{N}{2}$ quasielectrons over the $\frac{1}{3}$ state. At such high densities, the quasiparticles have a significant overlap so that the whole duality becomes questionable. In addition, for example the experimentally well-established $\frac{6}{13}$ requires 5 hierarchical steps in this hierarchy but is readily obtained in the composite-fermion picture. For such reasons, the Haldane-Halperin hierarchy is now largely replaced by the composite-fermion theory. For completeness, we include the

formula for computing the filling fractions in the Haldane-Halperin hierarchy

$$\nu = \cfrac{1}{m \pm \cfrac{1}{2p_1 \pm \cfrac{1}{2p_2 \pm \cfrac{1}{2p_3 \pm \cdots}}}} , \tag{1.1.26}$$

where p_k are positive integers, and for the kth hierarchical level, the continued fraction cuts after p_k. Importantly, after reduction, all fractions obtained this way have an odd denominator.

As pointed out at the beginning, currently the most interesting quasiparticles are believed to occur in the ground-state at filling fraction $\frac{5}{2}$. Unlike all other observed filling fractions in single-layer experiments, this one has an even denominator, and is therefore clearly inexplicable in either of the above presented pictures. Current understanding [21, 22, 23] is that the even denominator is achieved by pairing of composite-fermions by p-wave pairing (as opposed to the conventional s-wave pairing in usual superconductors), which generally leads to filling fraction $n + \frac{1}{2m}$ with n inert Landau levels and $2m$ attached flux quanta. Moreover, for a phase of weakly paired fermions, there is a domain wall between the weak pairing phase and empty space (which would be continuously connected to strong paired phase), which can have one zero-energy Majorana fermion mode that propagates along the domain wall. Similarly, associated with each well-separated vortex core (the density goes to zero at the vortex core), there is such a zero-energy mode, which makes the ground-state 2^{n-1}-fold degenerate. Adiabatic transport of the vortices then leads to unitary transformations within the degenerate ground-state subspace. Since the corresponding unitary matrices for different quasiparticle species turn out not to commute, the statistics of quasiparticles is non-Abelian [24]. More discussion from the point of view of Chern-Simons theory is presented in the next Chapter. For the time being, we merely write down the wave function for the ground-state of such a paired state suggested by Moore and Read [25],

$$\Psi_{\mathrm{MR}}(z_1, \ldots, z_N) = \mathrm{Pf}\left(\frac{1}{z_i - z_j}\right) \prod_{i<j} (z_i - z_j)^{2m} e^{-\sum_i z_i \bar{z}_i / 4l_c^2} . \tag{1.1.27}$$

The latter part of the wave function ought to be familiar from the composite-fermion theory. The Pfaffian factor, which comes from the projection of a BCS wave function to

N particles, is defined as the normalized antisymmetrized product over pairings, that is

$$\mathrm{Pf}(g_{ij}) = \frac{1}{2^{\frac{N}{2}}(\frac{N}{2})!}\epsilon^{i_1 i_2 \ldots i_N} g_{i_1 i_2} g_{i_3 i_4} \cdots g_{i_{N-1} i_N}, \tag{1.1.28}$$

and the normalization is such that $\mathrm{Pf}(g_{ij})^2 = \det(g)$.

In addition to $\frac{5}{2}$, there are quite a few other fractions that could, in principle, have quasiparticles with non-Abelian statistics [26]. Perhaps the second in line is the fragile state observed at $\frac{12}{5}$. According to some numerical work [27, 28] this state is very close to a phase transition between the Abelian hierarchy and a non-Abelian $\mathbb{Z}_3$ parafermion state, which would have even richer braiding properties than those of the Moore-Read state. Among the few other optimistic proposals [26] are the states at $\frac{4}{11}$, $\frac{8}{3}$ and $\frac{7}{3}$, although more conventional Abelian explanations have been made for all of them.

Before finishing this section, a comment about the spin is in order. The above quasiparticles were derived in the spin-frozen theory. In an actual sample, if the Zeeman effect is small, the quasiparticles may be skyrmions [9]. A skyrmion is continuously mapped to a vortex as the Zeeman effect increases, but an antiskyrmion is not continuously mapped to antivortex as they are composed mainly of opposite spin types. Throughout the reminder of this work, we assume that the electrons on the highest occupied Landau level are spin-polarized and use terms quasihole (quasielectron) and vortex (antivortex) interchangeably.

1.2 Anyons

In the introduction to quantum Hall effects, we already encountered quasiparticles, which accumulated an extra phase in addition to the Aharonov-Bohm phase when encircling other quasiparticles, and called the phenomenon fractional statistics. It is in order to present the modern generalized definition of quantum statistics [29, 30, 31, 32, 33] that may not be standard knowledge, on which these statements are based.

Feynman's path-integral formalism offers a particularly transparent viewpoint to quantum statistics [33]. The propagator for a system with N particles is written as the sum over all continuous paths in the configuration-space that connect the initial configuration ξ at time t to the final configuration ξ' at t'. For indistinguishable particles, the configurations that differ only by the permutation of particle indices should be identified. This solves the Gibbs paradox of statistical mechanics, namely that entropy does not change in the mixing of two identical fluids. Further requirement is that the configurations where particle co-

ordinates coincide (denoted by diagonal D) are forbidden. This is a crucial assumption, since without it the configuration-space would be simply connected, and in the following we would merely obtain the Bose statistics indicating that only bosons can be at the same space-time point. With the above assumptions, the configuration-space for N particles on a d-plane is then $M_N = (\mathbb{R}^{dN} - D)/S_N$, which is multiply connected for $N \geq 2$.

In a multiply connected configuration-space, the propagator decomposes according to the homotopy of different paths weighted by complex factors $\chi(\alpha)$

$$K(\xi', t', \xi, t) = \sum_{\alpha \in \pi_1(M_N)} \chi(\alpha) \int_{\xi(t) \in \alpha} \mathcal{D}\xi(t) \exp\left(i \int_{t'}^{t} \mathrm{d}t L\right) . \tag{1.2.1}$$

In the formula, we have already identified the homotopy classes of different paths with the first homotopy group, or the fundamental group, of the configuration-space M_N. This can be done by fixing a mesh of paths from a fixed base point ξ_0 to every point in M_N and adjoining the path $\xi\xi'$ with the mesh paths $\xi_0\xi$ and $\xi'\xi_0$ to form a loop. Invariance under different choices of mesh and the composition law of propagator imply that $\chi(\alpha)$ must be a phase factor that forms a representation of $\pi_1(M_N)$.

For $d \geq 3$, the loops can bypass the single punctures ($\pi_1(\mathbb{R}^{dN} - D) = \mathbf{1}$), so that the homotopy classes of M_N are dictated by the final permutation of particle positions, $\pi_1(M_N) = S_N$. The two U(1) representations are the trivial representation and the representation in which $\chi(\alpha) = \pm 1$ depending on the parity of the permutation. Thus, in $d \geq 3$ only Bose-Einstein and Fermi-Dirac statistics are allowed.

In two-dimensional space, the diagonal points D can no longer be bypassed, and $\pi_1(M_N)$ has a much more complex structure. In fact, it is isomorphic to the Artin's braid group $\mathcal{B}_N$ [34], which is an infinite dimensional non-Abelian group generated by $\{\sigma_i\}_{i=1}^{N-1}$ that satisfy the Artin relations: the commutation relation

$$\sigma_i \sigma_j = \sigma_j \sigma_i \quad (i \neq j \pm 1) , \tag{1.2.2}$$

and the Yang-Baxter relation

$$\sigma_i \sigma_{i+1} \sigma_i = \sigma_{i+1} \sigma_i \sigma_{i+1} . \tag{1.2.3}$$

The braid group is physically visualized by strands of particle wordlines that constantly move to the time-direction (by convention upwards). The σ_i corresponds to interchange of the strand at position i with the strand at $i + 1$ in an anti-clockwise manner.

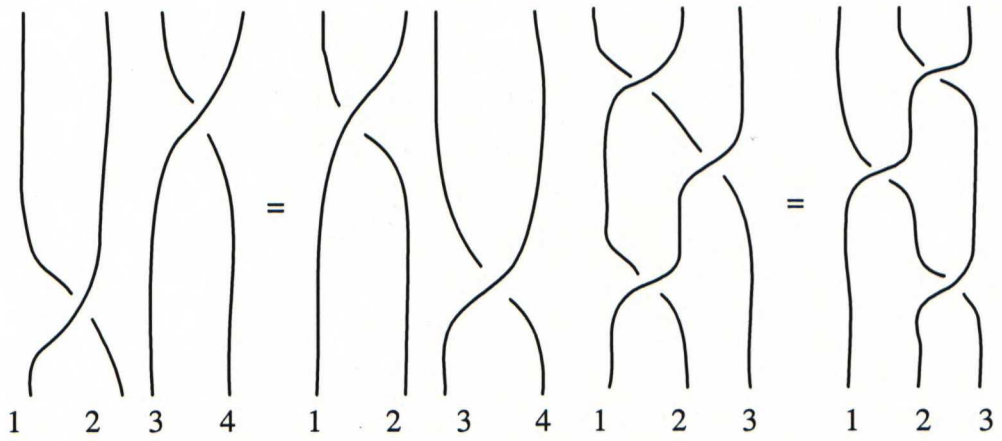

Figure 1.3: Braid diagrams for the Artin relations.

In Figure 1.3, the commutation relation and the Yang-Baxter relation are pictorially motivated with $N = 4$ and $N = 3$, respectively. The directions of the braids are kept track of by carefully distinguishing which strand passes over the other one.

Since one-dimensional unitary representations are all Abelian, the Artin relations for them reduce to $\chi(\sigma_i) = \chi(\sigma_{i+1})$, so that $\chi_\theta(\sigma_j) = e^{i\pi\theta}$ with arbitrary $\theta \in [0, 2)$ exhaust all the possibilities. Particles that transform as $e^{i\pi\theta}$ under braid are termed anyons, and their statistics can interpolate continuously 'any'thing between the bosonic and fermionic statistics. Let us further define $\theta_{ij}(t)$ to be the angle of particle i relative to particle j with respect to some fixed axis. In general, the weights $\chi(\alpha)$ in the propagator then become

$$\chi_\theta(\alpha) = \exp\left(i\theta \int_{t'}^{t} \mathrm{d}t \frac{d}{dt} \sum_{i<j} \theta_{ij}(t)\right) , \tag{1.2.4}$$

and the propagator itself can be rewritten as

$$K(\xi', t', \xi, t) = \int_{\xi(t)\in\mathbb{R}^{2N}-D} \mathcal{D}\xi(t) \exp\left(i \int_{t'}^{t} \mathrm{d}t \left[L + \theta \frac{d}{dt} \sum_{i<j} \theta_{ij}(t)\right]\right) , \tag{1.2.5}$$

in which the paths differing only by permutation of initial particle positions are included in the path-integral. The additional topological term in the action incorporates the fractional statistics. An alternative equivalent approach is to transfer the topological term directly into the wave function, thus resulting into multivalued wave functions for anyons. As an example, consider the wave function for two quasiholes at η_1 and η_2 in the Laughlin state

at $\nu = \frac{1}{2m+1}$

$$\Psi_{\eta_1\eta_2}(z_1,\ldots,z_N) = (\eta_1-\eta_2)^{\frac{1}{2m+1}}\prod_{i=1}^{N}(z_i-\eta_1)(z_i-\eta_2)\times$$
$$\prod_{i<j}(z_i-z_j)^{2m+1}\exp\left(-\frac{1}{4l_c^2}\left[\frac{1}{2m+1}(\eta_1\bar{\eta}_1+\eta_2\bar{\eta}_2)+\sum_{i=1}^{N}z_i\bar{z}_i\right]\right). \tag{1.2.6}$$

The fractional statistics is then obtained from the explicit monodromy of the wave function, and the corresponding Berry phase vanishes in this fractional statistics gauge [35].

An interesting possibility is that the topological term could be dynamically generated, and indeed, the fractional statistics of quasiparticles in the fractional quantum Hall effect suggests the realization of such a term with non-integer θ in an effective description of quasiparticles. In the field theoretic description, the topological term is a Chern-Simons term $\epsilon^{\mu\nu\rho}A_\mu\partial_\nu A_\rho$ with U(1) gauge field A (which we emphasize has nothing to do with the U(1) gauge field of electromagnetism) coupled to the quasiparticle current as seen in the following chapter.

Above, we were implicitly assuming that the wave function is a singlet, so that the representations of the Artin's braid group had to be one-dimensional, and hence Abelian. However, for a multiplet that can arise for example as a degenerate ground-state of emergent quasiparticles in a condensed matter system, the higher dimensional non-Abelian representations become possible. Chern-Simons terms for non-Abelian gauge fields with particle wordlines represented as Wilson lines are known to produce non-Abelian particle properties [36]. This is related to the fact that the correlation functions in some conformal field theories [37, 38] divide up to conformal blocks with nontrivial monodromy (analytic continuation around branch cuts) properties. The quantum Hall states obtained by interpreting the conformal blocks as wave functions then explicitly exhibit the non-Abelian statistics [26] in analogy to the explicit fractional statistics in Equation (1.2.6). These approaches are, although superficially, discussed in the next chapter in the context of the Moore-Read quantum Hall state suspected to explain the observed filling fraction $\nu = \frac{5}{2}$.

1.3 Quantum dots

Modern semiconductor processing techniques have enabled the manufacture of electronic nanostructures where the motion of electrons (or holes) is confined to small space in all three dimensions. Such systems are called (semiconductor) quantum dots. Typically, a low-temperature two-dimensional electron fluid in a semiconductor heterostructure is restricted to a finite area either laterally by electrostatic gates that lay on the surface or vertically by etching (see Figure 1.4). The shape of the confining potential can be tailored and electronic occupation of quantum dots can these days be tuned exactly at the precision of elementary charge.

The thickness of a dot relative to its lateral extent depends on the fabrication method and the applied gate voltages. However, as in the two-dimensional quantum Hall bars, a small extension of the electron wave function in perpendicular direction seems to be merely a change in the effective Coulomb interaction between the electrons. The metallic gates and point contacts used for measurements may further distort the interaction in the form of screening. The confining potential of quantum dot can usually be well treated in rotationally symmetric harmonic approximation even when the gates that form the confinement are rectangular. These considerations underlie our detailed model to be presented in Section 3.1.

As the shape of the confining potential can be adjusted, quantum dots provide remarkable control over individual electrons. The next step, control over individual spins, has already taken place and has numerous applications in quantum information processing [39]. The chaotic properties of quantum dots have been studied using methods such as the random matrix theory, the renormalization group, and $1/N$ expansion [40]. In this work, however, we are mainly interested in the electronic structure [41] of the quantum dots at the high magnetic field regime where the spins of the electrons are assumed polarized.

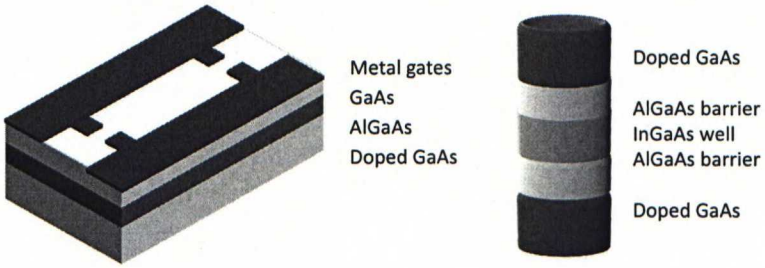

Figure 1.4: Example structures of a lateral and vertical quantum dot drawn after [41].

Chapter 2

Effective field theories

The trial wave function approach developed in the introduction does not give an entirely satisfactory theoretical account for the fractional quantum Hall effect. As for other phase transitions, one would like to identify an order parameter that tells when the FQHE phase is realized. However, to find such an order parameter for FQHE is difficult since the standard Landau-Ginzburg theory of symmetry breaking can not be employed when the phase transitions are not related to broken symmetries.

Historically, Girvin and MacDonald [42] suggested that the binding of flux to electrons should be viewed as a non-local order parameter for the Laughlin states. Moreover, they showed that applying a singular gauge transformation that binds $2m+1$ flux quanta to each electron turns the $\nu = \frac{1}{2m+1}$ Laughlin wave function into a bosonic wave function that contains off-diagonal long-range order, a characteristic of Bose condensation. The off-diagonal long-range order persisted for more realistic wave functions where the flux is only bound near the electrons. Filling fractions $\frac{1}{2m+1}$ could then be seen naturally as Bose-Einstein condensates of charge-flux composites. Based on this topological order parameter, Zhang, Hansson, and Kivelson [43] came up with a microscopic derivation of an effective field theory (Chern-Simons-Landau-Ginzburg theory) for the Laughlin states, in which the flux-binding is enforced by a U(1) gauge field in a topological Chern-Simons term. In an equivalent dual form of the theory [44], the quasiparticles are taken to be the fundamental fields, and the fractional statistics is enforced by a Chern-Simons term. Similar theories where then obtained by others [45, 46, 47, 48] for the Jain and Haldane-Halperin hierarchies. The situation is, however, more complicated for the quantum Hall states with non-Abelian quasiparticles as the corresponding Chern-Simons theory may

not be straightforwardly derived. Instead, the Chern-Simons theory is usually obtained through complicated path by first guessing a conformal field theory, which leads to realistic wave functions, and then deducing the Chern-Simons theory from the conformal field theory.

Related to the low-energy effective theories is the concept of universality classes. Systems that flow to the same infrared fixed point belong to the same universality class and are described by the same low-energy effective theory [49]. It is a compelling thought that different quantum Hall states could be classified in a wave function independent manner according to the low-energy properties, such as the edge excitations and the quantum numbers of quasiparticles, encoded in the effective low-energy theory. Progress in this direction has been made among others by Wen [49, 50, 51, 52] who has emphasized the importance of classifying topological orders of different universality classes in topological fluids.

In what follows, we formulate the effective theories for quasiparticles in the universality classes of the Laughlin states and Moore-Read state, discuss quasiparticle properties, and show how the spectrum of low-energy edge excitations that characterizes the topological order of the state arises in a finite quantum Hall system with a boundary.

2.1 U(1) Chern-Simons and bosonic edge modes

The effective Lagrangian for the universality class of Laughlin states in the dual form description of quasiparticles reads [26, 49]

$$\mathcal{L} = \frac{k}{4\pi}\epsilon^{\mu\nu\rho}a_\mu\partial_\nu a_\rho - \frac{1}{2\pi}\epsilon^{\mu\nu\rho}A_\mu\partial_\nu a_\rho - j^\mu_{\text{qp}}a_\mu \,. \tag{2.1.1}$$

The first term on the right is the Chern-Simons term, and the two remaining terms are coupling of the Chern-Simons field to the gauge potential A_μ of the electromagnetic field and the quasiparticle current j^{qp}_μ. The gauge potential of the magnetic field responsible for the Hall effect should not be included in A_μ as it is implicitly contained in the coefficient k. The presence of $\epsilon^{\mu\nu\rho}$ signals the violation of parity and time-reversal symmetries, which are broken due to the external magnetic field. Under a transformation $a_\mu \to a_\mu + \partial_\mu\Lambda$, the Chern-Simons term is invariant up to a total space-time derivative

$$\delta\mathcal{L}_{\text{CS}} = \frac{k}{4\pi}\partial_\mu(\Lambda\epsilon^{\mu\nu\rho}\partial_\nu A_\rho) \,, \tag{2.1.2}$$

and thus, if the manifold has no boundary or the boundary contribution is zero, a_μ is recognized as a U(1) gauge field. At the end of this subsection, we show how this boundary term is related to degrees of freedom at the boundary of a finite quantum Hall system, which manifest themselves as low-energy edge excitations.

Since the coupling of electromagnetic field to the electric current is in general of the form $-j^\mu A_\mu$, the electric current is given by

$$j^\mu = -\frac{\partial\mathcal{L}}{\partial A_\mu} = \frac{1}{2\pi}\epsilon^{\mu\nu\rho}\partial_\nu a_\rho \,, \tag{2.1.3}$$

from which the electronic density $\rho = \frac{1}{2\pi}\nabla\times\mathbf{a}$. To retrieve the conductivity, one can eliminate the Chern-Simons field by performing the functional integral over the a_μ field (since it is quadratic in action). One then finds the quantized Hall conductivity corresponding to filling fraction $\nu = \frac{1}{k}$. The requirement for k to be an odd integer follows initially from the fact that odd number of flux quanta must be attached to electrons to obtain a Bose condensate in the derivation of Chern-Simons-Landau-Ginzburg theory. In the dual form, this is equivalent with the condition that the matter field excitations corresponding to electrons have fermionic statistics.

We assume that the quasiparticles move along predetermined classical trajectories,

which determine j_μ^{qp}. The equations of motion corresponding to variation of a_μ are

$$\frac{k}{2\pi}\epsilon^{\mu\nu\rho}\partial_\nu a_\rho = j^\mu_{\text{qp}} + \frac{1}{2\pi}\epsilon^{\mu\nu\rho}\partial_\nu A_\rho \,. \tag{2.1.4}$$

We fix the gauge by $a_0 = 0$ so that the zeroth component of this equation is the Chern-Simons constraint

$$k\rho = \frac{k}{2\pi}\nabla \times \mathbf{a} = \rho_{\text{qp}} + \frac{1}{2\pi}B \,. \tag{2.1.5}$$

Hence the quasiparticles have charge $\frac{1}{k}$ times the electric charge and each quasiparticle binds a Chern-Simons flux $\frac{2\pi}{k}$. When one quasiparticle is taken around another through path C corresponding to a double interchange, the action is equal to $\int_C \mathrm{d}\mathbf{r}\cdot\mathbf{a}$ that is just the Chern-Simons flux of the enclosed quasiparticle $\frac{2\pi}{k}$. The quasiparticles obey the fractional statistics as they should for the Chern-Simons theory to correctly describe the macroscopic topological properties of the Laughlin states.

Let us now return to the boundary term (2.1.2) and derive a neat result, important for the computations of this thesis. As we are, by assumption, considering long-distance physics, we may take the boundary to be the x-axis so that the fields are defined at $y \leq 0$. The boundary terms in x- and t-direction then vanish, and after integrating over y we are left with

$$\delta S_{\text{CS}} = \frac{k}{4\pi}\int_{y=0} \mathrm{d}x\mathrm{d}t\Lambda(\partial_t a_x - \partial_x a_t) \,. \tag{2.1.6}$$

To have a self-consistent gauge invariant theory, we define the effective theory for a system with boundary by restricting gauge transformations to be zero at the boundary $\Lambda|_{y=0} = 0$. We may fix the gauge by setting $a_t = 0$, and imposing the constraint

$$\frac{\partial \mathcal{L}_{\text{CS}}}{\partial a_t} = \frac{k}{2\pi}\epsilon^{ij}\partial_i a_j = 0 \,. \tag{2.1.7}$$

Since the curl of the remaining gauge potential is zero, it can be expressed as a gradient of a scalar field as $a_i = \partial_i\phi$. Substitution to Chern-Simons action and integration over y (there is a total space derivative) gives an action defined on the boundary

$$S_{\text{CS}} = -\frac{k}{4\pi}\int \mathrm{d}x\mathrm{d}t\phi\partial_t\partial_x\phi_x = \frac{k}{4\pi}\int \mathrm{d}x\mathrm{d}t\partial_t\phi\partial_x\phi \,. \tag{2.1.8}$$

One can easily check that the Hamiltonian for this action is zero. This is because we have not fixed the velocity of the edge modes relative to the laboratory frame, always present in real experiments. In order to do this, we write ϕ in terms of the physical field

$\tilde{\phi}(x - vt, t) = \phi(x, t)$, where v is the velocity of the edge modes that depends on the details of the boundary. The action is then

$$S_{\text{CS}} = \frac{k}{4\pi} \int \mathrm{d}x\mathrm{d}t(\partial_t - v\partial_x)\tilde{\phi}\partial_x\tilde{\phi} \,, \tag{2.1.9}$$

which is a chiral boson theory. Dropping tildes in the following, the canonical momentum becomes $\pi = \frac{k}{4\pi}\partial_x\phi$ and the Hamiltonian is written as

$$H = \int \mathrm{d}x \left(\pi\dot{\phi} - \mathcal{L}_{\text{CS}}\right) = \frac{kv}{4\pi} \int \mathrm{d}x(\partial_x\phi)^2 \,. \tag{2.1.10}$$

The condition for Hamiltonian to be bounded from below implies $kv > 0$, that is, the magnetic field that causes the Hall effect determines the direction of the chirality, the sign of v. The chiral boson theory is quantized by imposing commutation relations [49]

$$\begin{aligned} [\pi(x), \phi(x')] =& \frac{i}{2}\delta(x - x') \,, \\ [\phi(x), \phi(x')] =& \frac{\pi}{k} \operatorname{sgn}(x - x') \,. \end{aligned} \tag{2.1.11}$$

To identify the spectrum of the theory given by Equations (2.1.10) and (2.1.11), we define $\rho = \frac{1}{2\pi}\partial_x\phi$ and go to Fourier space:

$$\rho_q = \frac{1}{\sqrt{L}} \int \mathrm{d}x e^{iqx}\rho(x) \,, \tag{2.1.12}$$

where $q \in \{2\pi n/L \mid n \in \mathbb{Z} - 0\}$ and L is the length of the boundary. In terms of the new variables the Hamiltonian reads

$$H = k\pi v \int \mathrm{d}x\rho^2 = 2\pi vk \sum_{q>0} \rho_q\rho_{-q} \,, \tag{2.1.13}$$

and the commutation relations are deduced by

$$\begin{aligned} [\rho_q, \rho_{q'}] &= \frac{1}{(2\pi\sqrt{L})^2} \left[\int \mathrm{d}x e^{iqx}\partial_x\phi(x), \int \mathrm{d}x' e^{iq'x'}\partial_{x'}\phi(x')\right] \\ &= \frac{-i}{k\pi L} \int \mathrm{d}x\mathrm{d}x' e^{i(qx+q'x')} q'[\pi(x), \phi(x')] = \frac{q\delta_{q+q'}}{2\pi k} \,. \end{aligned} \tag{2.1.14}$$

The algebra of ρ_q in Equation (2.1.14) is known as the U(1) Kac-Moody algebra. The Hamiltonian (2.1.13) describes a set of uncoupled oscillators. If the system is bounded to a disk, the different modes can be identified as the modes with different angular momentum. The number of edge states corresponding to a total angular momentum ΔM on the

edge is nothing but the combinatoric number that tells how many ways angular momenta $1, 2, \ldots, \Delta M$ can be added to obtain ΔM, that is, the partition of ΔM. For example,

$$\begin{aligned} 1 \\ 2 = 1+1 \\ 3 = 2+1 = 1+1+1 \\ 4 = 3+1 = 2+2 = 2+1+1 = 1+1+1+1 \end{aligned} , \tag{2.1.15}$$

so that the number of edge modes with angular momenta $\Delta M = 1, 2, 3,$ and 4 are 1, 2, 3, and 5, respectively.

An alternative way to look at the edge excitations is offered by the theory of symmetric polynomials. We define a positive semidefinite Hamiltonian that gives zero-energy for exactly those wave functions that vanish as $\mathcal{O}((z_i - z_j)^{2m+1})$ when electrons i and j are brought together (the explicit form of the Hamiltonian is given in Section 3.2). Then, the Laughlin state at $\nu = \frac{1}{2m+1}$ is the lowest angular momentum zero-energy state, and all other zero-energy states corresponding to higher angular momenta are obtained by multiplying it with a symmetric polynomial. The number of symmetric polynomials of degree ΔM is exactly the partition of ΔM [53]. Thus, the edge modes can be identified as the Laughlin states multiplied by the symmetric polynomials. For only a finite number of electrons the arguments of the symmetric polynomials are restricted to a finite number, and hence some of the modes become linearly dependent. The number of symmetric polynomials of N arguments are given by the N-restricted partitions [53], that is the number of ways ΔM can be formed by summing $1, 2, \ldots, N$. These are the numbers of edge excitations in a finite small system such as a quantum dot. The number of edge modes are summarized in Table 2.1 for small electron numbers and at the thermodynamic limit.

Table 2.1: Number of edge states of the Laughlin states with angular momentum ΔM for different bulk electron numbers N.

ΔM	0	1	2	3	4	5	6	7	8	N
	1	1	2	2	3	3	4	4	5	2
	1	1	2	3	4	5	7	8	10	3
	1	1	2	3	5	6	9	11	15	4
	1	1	2	3	5	7	10	13	18	5
	1	1	2	3	5	7	11	14	20	6
	1	1	2	3	5	7	11	15	21	7
	1	1	2	3	5	7	11	15	22	8
	1	1	2	3	5	7	11	15	22	∞

2.2 SU(2) Chern-Simons and Majorana fermions

The Chern-Simons term in the previous section is generalized for non-Abelian theories as [1]

$$\mathcal{L}_{\mathrm{CS}} = \frac{k}{4\pi}\epsilon^{\mu\nu\rho}\,\mathrm{tr}\left(a_\mu\partial_\nu a_\rho + \frac{2}{3}a_\mu a_\nu a_\rho\right), \tag{2.2.1}$$

where the gauge field $a_\mu = a_\mu^a t^a$ takes values in a finite dimensional representation, generated by the matrices t_a, of a semi-simple Lie algebra G. Coupling constant k is referred to as the level, and the corresponding theory is denoted G_k. Under the transformation $a_\mu \to g^{-1}a_\mu g + g^{-1}\partial_\mu g$, where $g \in G$, the Chern-Simons term changes by

$$\delta L_{\mathrm{CS}} = \frac{k}{4\pi}\epsilon^{\mu\nu\rho}\partial_\mu \mathrm{tr}(\partial_\nu g g^{-1}A_\rho) - \frac{k}{12\pi}\epsilon^{\mu\nu\rho}\,\mathrm{tr}(g^{-1}\partial_\mu g g^{-1}\partial_\nu g g^{-1}\partial_\rho g)\,. \tag{2.2.2}$$

The first term, a total space-time derivative, is treated just as in the Abelian case. The second term can be written in terms of the winding number density $w(g)$ of the group element g as $-2\pi k w(g)$ since [1]

$$w(g) = -\frac{1}{24\pi^2}\epsilon^{\mu\nu\rho}\,\mathrm{tr}(g^{-1}\partial_\mu g g^{-1}\partial_\nu g g^{-1}\partial_\rho g)\,. \tag{2.2.3}$$

With appropriate boundary conditions the integral of $w(g)$ is an integer, so that the quantity $\exp(iS_{\mathrm{CS}})$ is gauge invariant if k is an integer (even though $\mathcal{L}_{\mathrm{CS}}$ alone is not invariant).

The effective field theory describing the universality class of the Pfaffian quantum Hall state [21] contains a $G_k = \mathrm{SU}(2)_2$ Chern-Simons term, which is responsible for the

non-Abelian statistics of the quasiparticles. In addition, there is an abelian Chern-Simons field effect of which amounts to a phase factor in the braiding matrices. There are two common ways to derive the quasiparticle properties from the Chern-Simons theory [26], though both of them are too lengthy to be discussed here in detail.

In the first approach that does not rely on any particular gauge, one includes the quasiparticles that move along classically prescribed trajectories into the Lagrangian according to $\mathcal{L} = \mathcal{L}_{\mathrm{CS}} + \mathrm{tr}(j_{\mathrm{qp}} \cdot a)$. By studying the Chern-Simons term on a manifold of $n+1$-punctured sphere and relating quasiparticles to the punctures, one finds that the number of different species of quasiparticle-quasihole pairs is $k+1$, with k the level of the theory defined above. Moreover, all the other quasiparticles are obtained by fusing several quasiparticles of a special type, say type σ. A source term that describes the creation, propagation, and annihilation of a quasiparticle-quasihole pair along trajectories defining a loop γ is incorporated into the path integral as a gauge invariant Wilson loop [54]

$$W_\gamma[a] = \mathrm{tr}\left[\mathcal{P}\exp\left(i\oint_\gamma \mathrm{d}x^\mu a_\mu^a t^a\right)\right] , \tag{2.2.4}$$

where $\mathcal{P}$ is the path-ordering operator. In the presence of several such loops, which form a link L, the vacuum to vacuum amplitude for the process is written as

$$\langle 0|0\rangle_{\gamma_1,\ldots,\gamma_n} = \int \mathcal{D}a W_{\gamma_2}[a]\ldots W_{\gamma_n}[a]e^{iS_{\mathrm{CS}}[a]} . \tag{2.2.5}$$

One then uses the remarkable result by Witten [36], namely that the path-integral above is nothing but the Jones polynomial [55] V_L associated with the link L evaluated with the argument $-e^{i\pi/k+2}$. By evaluating the Jones polynomial for various links, one then finds the fusion rules and the non-Abelian statistics of the quasiparticles.

The second approach is to consider the Chern-Simons theory in a specific gauge. One then finds that the gauge-fixed 2+1-dimensional Chern-Simons action can be viewed as the partition function of a 2+0-dimensional Wess-Zumino-Witten model [56, 57]. For positive integers k, the WZW model is two-dimensional conformal field theory, and thus one can utilize the strong nonperturbative machinery that is special for two-dimensional conformal field theories (only then is the group of conformal transformations, isomorphic to group of analytic functions, infinite-dimensional). One can then derive the wave functions in the presence of quasiparticles from the conformal field theory, and the non-Abelian statistics is automatically entailed in the monodromy properties of the wave functions.

As in the previous section, the edge spectrum can be derived by taking a boundary condition that restricts the gauge transformations on the boundary to identity. One can

then fix the gauge, as above, after which one ends up with the same WZW conformal field theory. Since the action only depends on the values of the fields at the boundary, the transformations in the bulk that are independent of the co-ordinate along the boundary are the global symmetries of the theory. The edge spectrum can be organized into the representations of the corresponding symmetry group, which in the case of WZW model would lead one to consider the Virasoro algebra and representations of the G_k Kac-Moody algebra. The $SU(2)_2$ WZW model is a triplet of chiral Majorana fermions. Because of the Abelian Chern-Simons field present in the effective action of the Pfaffian state, two chiral Majorana fermions are actually composed to form a chiral boson. Therefore, the edge theory of the Pfaffian state is a combination of a chiral boson and a chiral Majorana fermion. In fact, a quantum Hall state will always have a chiral boson term in its effective edge theory, since the U(1) symmetry is responsible for the charge conservation and thus of the edge excitations that carry the quantized Hall current. More details in [26]. We next derive the spectrum of edge excitations of the Pfaffian state, starting from the theory of a chiral Majorana fermion.

The chiral Majorana fermion has the Lagrangian [58]

$$\mathcal{L} = i\psi(\partial_t - v\partial_x)\psi \,, \tag{2.2.6}$$

where ψ is a real fermion field $\psi^\dagger = \psi$. The canonical momentum is evaluated to be $\pi = i\psi$, so the Hamiltonian becomes

$$H = \int \mathrm{d}x \left(\pi\dot{\psi} - \mathcal{L}\right) = iv \int \mathrm{d}x \psi\partial_x\psi \,. \tag{2.2.7}$$

The theory is quantized by setting $\{\pi(x), \psi(x')\} = i\delta(x - x')$, which is the same as $\{\psi(x), \psi(x')\} = \delta(x - x')$. Let us quantize the theory on a circle $x \in [0, 2\pi)$. Since ψ is real, the two alternate boundary conditions are $\psi(0, t) = \pm\psi(2\pi, t)$. Depending on the signature of the boundary condition, they are called the periodic (or $+$) boundary condition and the antiperiodic (or $-$) boundary condition.

We pass to the Fourier space by setting

$$\psi(x) = \frac{1}{\sqrt{2\pi}} \sum_q a_q e^{iqx} \,, \tag{2.2.8}$$

which has the inverse

$$a_q = \frac{1}{\sqrt{2\pi}} \int_0^{2\pi} \mathrm{d}x \psi(x) e^{-iqx} \,. \tag{2.2.9}$$

The values of q are determined by the boundary condition. For the periodic boundary condition $q \in \mathbb{Z}$, and for the antiperiodic boundary condition $q \in \{k + \frac{1}{2} \mid k \in \mathbb{Z}\}$. Using (2.2.9) with the anticommutation relation for ψ we readily find $\{a_q, q_{q'}\} = \delta_{q+q'}$. Substitution of (2.2.8) into the Hamiltonian (2.2.7) yields

$$H = v \sum_{q>0} q a_q a_{-q} \,, \tag{2.2.10}$$

which describes uncoupled fermionic modes propagating with different momenta. The symmetry $\psi \to -\psi$ of the Lagrangian (2.2.6) results in to the conservation of the parity of the fermion number $N_\psi = \sum_{q \geq 0} a_q a_{-q}$. Thus, the theory divides into four distinct sectors: (+,even), (−,even), (+,odd), and (−,odd). The number of states at each total momentum can now be calculated sectorwise. We denote the momentum relative to the ground-state by Δq. For example, in the even N_ψ sector with antiperiodic boundary conditions, the number of states at $\Delta q = n$ is the number of ways summing an even combination of $\frac{1}{2}, \frac{3}{2}, \frac{5}{2}, \ldots$ yields n. Thus, for $\Delta q = 0$ we only have the state with $N_\psi = 0$, for $\Delta q = 1$ we have nothing and after that,

$$\begin{aligned} 2 &= \frac{1}{2} + \frac{3}{2} \\ 3 &= \frac{1}{2} + \frac{5}{2} \\ 4 &= \frac{1}{2} + \frac{7}{2} = \frac{3}{2} + \frac{5}{2} \\ 5 &= \frac{1}{2} + \frac{9}{2} = \frac{3}{2} + \frac{7}{2} \\ 6 &= \frac{1}{2} + \frac{11}{2} = \frac{3}{2} + \frac{9}{2} = \frac{5}{2} + \frac{7}{2} \end{aligned} \,. \tag{2.2.11}$$

The number of states in each sector of the chiral Majorana fermion system is summarized in Table 2.2. Once the circle is embedded into a plane, the momentum change Δq along the circle can be identified as the angular momentum change ΔM.

As the edge theory of the Moore-Read state is a combination of a chiral Majorana fermion and a chiral boson

$$\mathcal{L}_{\partial \mathrm{Pf}}(\psi, \phi) = \mathcal{L}_{\text{Maj. fermion}}(\psi) + \mathcal{L}_{\text{boson}}(\phi) \,, \tag{2.2.12}$$

where the two are described by the Lagrangians (2.2.6) and (2.1.9), respectively. As the fermionic and bosonic modes are uncoupled, the number of states at each ΔM can be

Table 2.2: The number of states of the chiral Majorana fermion at each total q for the antiperiodic and periodic even and odd sectors.

Δq	0	1	2	3	4	5	6	7	8	b.c.	N_ψ
	1	0	1	1	2	2	3	3	5	−	even
	1	1	1	1	2	2	3	4	5	−	odd
	1	1	1	2	2	3	4	5	6	+	both

obtained straightforwardly. For example, consider $\Delta M = 3$ in the (−,even) sector. We have

$$\bar{3} = \bar{2} + \bar{1} = \bar{1} + \bar{1} + \bar{1} = \bar{1} + \frac{1}{2} + \frac{3}{2} = \frac{1}{2} + \frac{5}{2}, \tag{2.2.13}$$

where the angular momenta of bosonic modes are specified by a bar, and hence the number of states is 5. The number of edge states of the Pfaffian are summarized in Table 2.3.

Table 2.3: The number of edge states of the Pfaffian state at angular momenta ΔM relative to the ground-state.

ΔM	0	1	2	3	4	5	6	7	8	b.c.	N
	1	1	3	5	10	16	28	43	70	−	even
	1	2	4	7	13	21	35	55	86	−	odd
	1	2	4	8	14	24	40	64	100	+	both

Chapter 3

Numerical methods

Microscopic model of a quantum dot in a high magnetic field with external perturbations is introduced and motivated. After that, the computational methods, exact diagonalization, and numerical adiabatic time evolution of the many-body quantum state, are presented.

3.1 Microscopic model

We consider a semiconductor heterostructure, where electrons are confined to a plane and subjected to a perpendicular magnetic field $\vec{B} = B\vec{e}_z$. The planar electrons are further confined to a disk geometry by a potential that can be treated in the harmonic approximation. The Hamiltonian for N electrons interacting through Coulomb potential reads

$$H = \sum_{i=1}^{N} \left[\frac{1}{2m^*} (\vec{p}_i + e\vec{A}_i)^2 + \frac{1}{2} m^* \omega_0^2 r_i^2 \right] + \sum_{i<j} \frac{e^2}{4\pi\epsilon r_{ij}} , \tag{3.1.1}$$

where $m^* = 0.067 m_e$ is the effective mass [59] of the electron, and $\epsilon = 12.7\epsilon_0$ is the permittivity in a GaAs/AlGaAs interface. In the exact diagonalization studies of quantum Hall effect, it is common in literature to perform the computations in a boundaryless system, such as a sphere or torus. This avoids the edge effects that cause problematic radial density fluctuations for small particle numbers and thus allows for a much better approximation to the thermodynamic limit where the density is uniform. However, the edge modes frequently reflect the topological order of the ground-state obtainable by simply counting states. This is particularly true for the fictive model interaction potentials, which have exactly degenerate zero-energy states for the edge excitations, but also, though not so clearly, for the more realistic interactions presented below. Though the number of electrons in a quantum dot can range from one to hundreds, we consider here few-electron quantum dots accessible to our numerical methods.

The parabolic confinement potential is especially convenient in that the single-particle states are those encountered in the introduction with merely a redefinition of the length scale. However, the degeneracy of the Landau levels is lifted by the confinement, so that the solution of the interacting system is a specific angular momentum eigenstate. The Landau levels still form bands that narrow and separate from each other with the increasing magnetic field as seen in Figure 3.1. Tracing through the steps in the derivation of the eigenfunctions in (1.1.9), it is easy to verify that the single-particle states of the model (3.1.1) in symmetric gauge are

$$\psi_{nl}(z) = \sqrt{\frac{n!}{\pi(n+l)!}} z^l L_n^l(z\bar{z}) e^{-z\bar{z}/2} , \tag{3.1.2}$$

where z is now in the units where the oscillator length $l = \sqrt{\hbar/m^*\omega} = 1$ (note that index l is denoted by the same symbol) with the frequency $\omega = \sqrt{\omega_0^2 + (\omega_c/2)^2}$. The

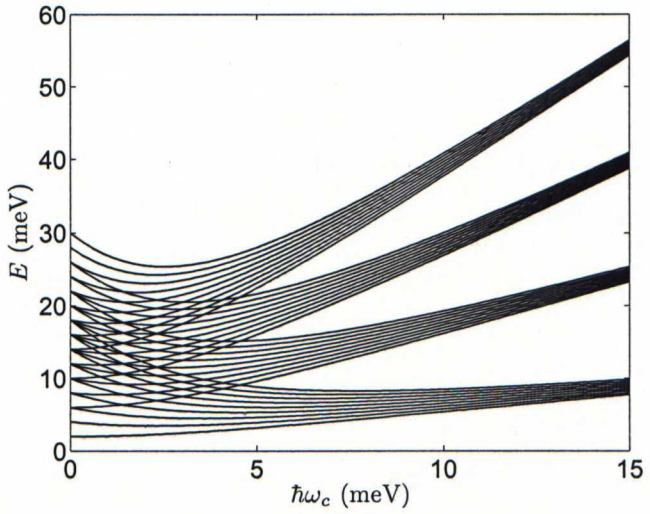

Figure 3.1: The non-degenerate Landau levels in a quantum dot. Lowest states on the four lowest Landau levels shown with $\hbar\omega_0$ =2 meV.

corresponding energies are

$$E_{nl} = (2n+1)\hbar\omega + l\left(\hbar\omega - \frac{\hbar\omega_c}{2}\right), \tag{3.1.3}$$

and they reduce to $(n+\frac{1}{2})\hbar\omega_c$ for $w_0 = 0$.

In an actual sample, the electrons are not strictly confined to two dimensions, and the sample width can have signicant effect on the effective interelectron interaction. Furthermore, nearby metallic layers can cause screening of the interaction. It is of interest to investigate the effects of these factors to the ground-state properties. It has been suggested that the excitation gap of a given quantum Hall state could be increased by designing the precise form of the interaction potential utilizing the above factors as well as the spin-orbit coupling [26, 60]. However, in such approaches it is crucial to maintain low enough level of disorder (for large enough gap), which no doubt causes complications. In general, the effective potentials due to finite layer thickness can be obtained by assuming a specific form for the wave functions in the z-direction and integrating over z. Qualitatively, they all lead to the softening of the Coulomb potential at short distances, and the simplest potential that has the property is

$$V(r) = \frac{e^2}{4\pi\epsilon}\frac{1}{\sqrt{r^2+l_i^2}}, \tag{3.1.4}$$

where l_t is proportional to the thickness of the electron layer. For a screened Coulomb interactions with characteristic screening scale l_s, we use potential

$$V(r) = \frac{e^2}{4\pi\epsilon r} \exp\left(-\frac{r^2}{l_s^2}\right) . \tag{3.1.5}$$

The effects may be combined to

$$V(r) = \frac{e^2}{4\pi\epsilon\sqrt{r^2 + l_t^2}} \exp\left(-\frac{r^2}{l_s^2}\right) , \tag{3.1.6}$$

though the additional results seem not to lead to qualitatively new features. The matrix elements for the above interactions used in the diagonalization of the Hamiltonian are mostly computed analytically (the results are combinations of hypergeometric functions and gamma functions), though on the second Landau level we resort to accurate numerical Romberg integration for the interactions (3.1.4) and (3.1.5). The detailed analytic calculations for the pure Coulomb interaction can be found in Refs. [61] and [62].

In the application of quantum Hall quasiparticles to topological quantum computation, the braiding is achieved by physically moving the quasiparticles around the sample in micrometer scale. This is achieved by localizing the quasiparticles to impurities, small gates, or the potential induced by tips of scanning microscopes. While a topological quantum computer may not be realized in a quantum dot geometry as the topological properties, by which we mean fractional and non-Abelian statistics become robust only for well separated quasiparticles, which require system of thousands of electrons, the trapping of the quasiparticles in a few electron droplets may still be interesting and enlightening, after all, the local trapping may not be as sensitive to the electron number, or equivalently length scale, as the non-local topological properties. To localize a quasiparticle at location η, we employ gaussian potential

$$V_T(z) = We^{-(z-\eta)^2/2s^2} . \tag{3.1.7}$$

The scale of the potential may be adjusted to bind quasielectrons (quasiholes) with negative (positive) W. The range of the potential is determined by s, and at the limit $s \to 0$ V_T reduces to a delta function potential. Several potentials may be used to create multiple quasiparticle excitations. However, if the trapping potential breaks rotational invariance ($\eta \neq 0$), the number of basis states needed for the solution increases rapidly, and despite effective algorithms not as many electrons can be afforded. Since we are already running out of electron density, we concentrate on quasihole excitations, whence the wavefunctions are also more amenable for investigations.

3.2 Landau level projection

At a high magnetic field $\omega_c \gg \omega_0$ and low temperature $\hbar\omega_c \gg kT$, processes that do not conserve the Landau level index can be neglected. Landau levels decouple, the filled Landau levels become inert, and the interesting dynamics occurs only in the Landau level directly above them, which for fractional filling factor is partially occupied. When a set of N particles have the same Landau level index, the remaining dynamical variables are the guiding center co-ordinates [63]

$$X_i^\alpha = x_i^\alpha + \epsilon^{\alpha\beta} p_i^\beta \,, \tag{3.2.1}$$

$\alpha \in \{1, 2\}$ and i is the particle index. These commute with the dynamical momentum

$$p_i^\alpha = -i\partial_i^\alpha + A_i^\alpha \,, \tag{3.2.2}$$

but the X and Y guiding co-ordinates of a particle are noncommutative

$$[X_i^\alpha, X_j^\beta] = -i\delta_{ij}\epsilon^{\alpha\beta} \,. \tag{3.2.3}$$

In fact, large part of quantum Hall physics is now understood in terms of noncommutative geometry [9]. When a potential term is applied to a state vector on a given Landau level, part of the resultant state in general no more resides on the same Landau level and that part is project out when a matrix element is computed. Thus, matrix elements of the Hamiltonian on a given Landau level contain redundant information. With the use of guiding centers, Haldane [63] has shown that the interaction energy of electrons residing single Landau level and interacting through rotational invariant interaction can be written as

$$H_V = \sum_{i<j} \sum_{m=0}^{\infty} V_m P_m(M_{ij}) \,, \tag{3.2.4}$$

where $P_m(M_{ij})$ is the projection operator to the relative angular momentum state M_{ij} between particles i and j, and V_m are the pseudopotential coefficients, which for Landau level n are given in terms of the Fourier transform $V(\mathbf{q})$ of the interaction potential by

$$V_m = \int_0^\infty \mathrm{d}q q V(q) \left[L_n(q^2/2)\right]^2 L_m(q^2) e^{-q^2} \,. \tag{3.2.5}$$

For spin-polarized fermions, due to the Pauli principle only terms with odd m are relevant. Simon et al. [64] have also generalized the pseudopotential construction for general multiparticle interactions.

With the pseudopotentials, an interaction Hamiltonian with a given Laughlin state as the lowest angular momentum zero-energy state is readily constructed. If the coefficients V_m are non-zero for $m \leq k$ and zero for $m \geq k$, then the Laughlin state for $\nu = \frac{1}{k}$ is exact zero-energy eigenstate, since in it all pairs of particles have relative angular momentum k. For computational purposes, the interaction may be written in real space as [49]

$$H_{\mathrm{L}} = -\sum_{i<j} \sum_{m=1}^{(k-1)/2} C_m \partial_{\bar{z}_i}^{2m-1} \delta(z_i - z_j) \partial_{z_i}^{2m-1} , \tag{3.2.6}$$

with positive constants C_m. Similarly, a careful analysis shows that the Paffian wave function at $\nu = \frac{1}{2}$ can be realized as [65, 66]

$$H_{\mathrm{Pf}} = -\sum_{i<j<k} S_{ijk}[\nabla_i^2 \nabla_j^2 (\nabla_i^2 + \nabla_j^2) \delta(z_i - z_j) \delta(z_i - z_k)] , \tag{3.2.7}$$

where $S_{ijk}[f_{ijk}] = f_{ijk} + f_{kij} + f_{jki}$ is the symmetrizer. Up to an irrelevant normalization, the matrix elements of H_{Pf} and H_{L} were used to obtain the exact Laughlin and Pfaffian wave functions in the exact diagonalization, as they were compared to the results obtained with the realistic Coulomb interactions. Detailed formulas for these matrix elements (for $k = 3$ in the former) can be found in the recent thesis, Ref. [67].

The Haldane pseudopotential coefficients characterize interaction at different ranges. In particular, the V_m with small m characterize the short-range part of the interaction. We next compare the pseudopotential coefficients of Coulomb interaction for different Landau levels, screening, and thickness. The V_m for the three lowest Landau levels are evaluated from Formula (3.2.5)

$$\begin{aligned} V_m^{\mathrm{LLL}} &= \frac{\pi \Gamma(m + \frac{1}{2})}{\Gamma(m+1)} , \\ V_m^{\mathrm{SLL}} &= \frac{\pi(8m-3)(8m-11)\Gamma(m-\frac{3}{2})}{64\Gamma m + 1} , \\ V_m^{\mathrm{TLL}} &= \frac{\pi(128m^2 - 608m + 585)(128m^2 - 352m + 105)\Gamma(m - \frac{7}{2})}{16384\Gamma(m+1)} , \end{aligned} \tag{3.2.8}$$

and are visualized in Figure 3.2. Importantly, the ratio V_1/V_3 decreases for higher Landau levels, which implies that the lowest Landau level is the most stable for the Laughlin state at filling $\frac{1}{3}$. Consider now the effect of finite-thickness of the electron layer. The V_m for the lowest Landau level are shown in Figure 3.3 for various thicknesses, and obviously the qualitative behaviour is the same for the higher Landau levels. Increasing thickness

continously changes the interaction to form of the higher Landau levels. Screening, on the other hand, naturally increases the short-range nature of the interaction, and has thus strong effect on the coefficients (see Figure 3.4). For sufficiently strong screening the interaction turns to the model interaction, which has Laughlin states as exact ground-states. Notice, however, the weakening of the interaction strength, which decreases the excitation gap, while the experimentally observed filling fractions have a large excitation gap.

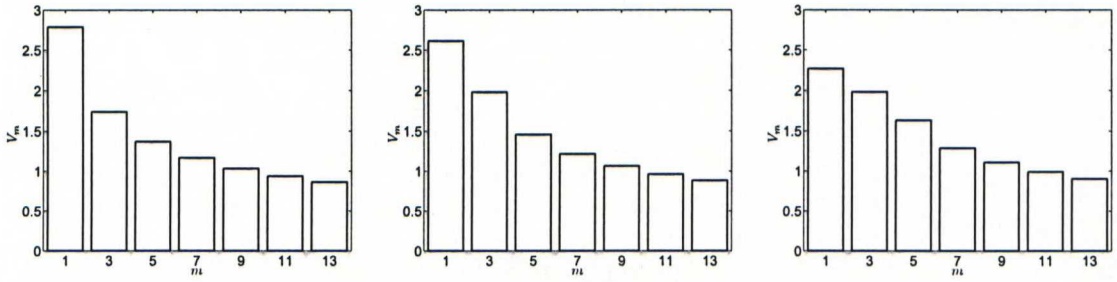

Figure 3.2: The Haldane pseudopotential coefficients for pure Coulomb interaction on the three lowest Landau levels (from left to right).

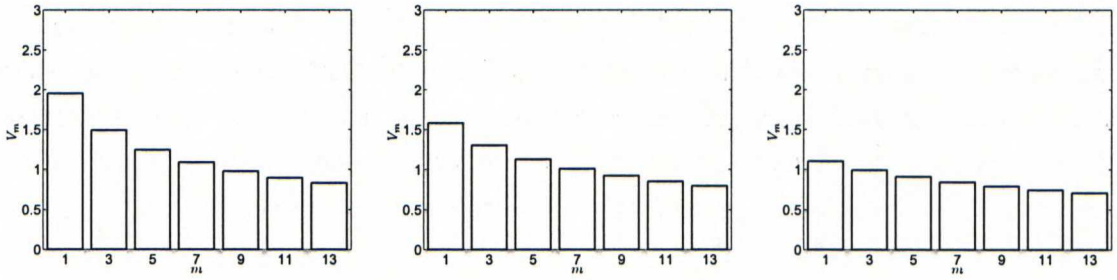

Figure 3.3: The lowest Landau level pseudopotential coefficients for finite-thickness Coulomb interaction with $d_t = 3$, 5 and 10 in units of l.

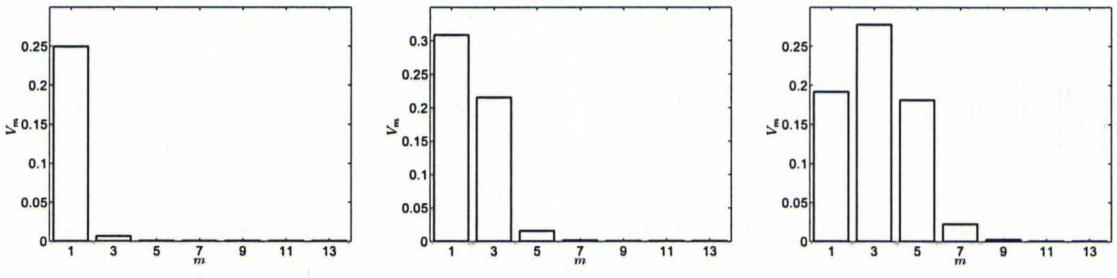

Figure 3.4: The pseudopotential coefficients for screened Coulomb interaction on three lowest Landau levels with characteristic screening length $d_t = 1$ in units of l.

3.3 Exact diagonalization

Exact diagonalization is a straighforward method to solve the eigenvalues and vectors of a Hermitian operator. Given a complete orthonormal discrete basis for the domain of the operator, which necessarily exists for a Hilbert space, we write the operator as a matrix in that basis. If the number of basis functions is small enough relative to the number of nonzero matrix elements of the operator, the matrix may be diagonalized either partially or fully, and the eigenvalues and eigenvectors are thus obtained. It may be that the matrix is infinite dimensional or otherwise too large, in which case the basis size needs to be reduced and the obtained results are then only approximate. In the quantum mechanical many-body problems, the number of particles needs to be set small enough, as the Hilbert spaces grows exponentially with the particle number.

We are solving the time-independent Schrödinger equation

$$H|\Psi\rangle = E|\Psi\rangle \,, \tag{3.3.1}$$

where H is defined by the model presented at the beginning of this chapter. The boundary condition for fermions is that the wave function $\Psi(z_1, z_2, \ldots, z_N) = \langle z_1, z_2, \ldots, z_N|\Psi\rangle$ must be antisymmetric under interchange of co-ordinates. It is most transparent to work in the second quantized picture. We perform the Landau level projection by taking the single-particle solutions (3.1.2) for fixed n as the single-particle basis $\{|i\rangle\}$. Hamiltonian containing one-body, two-body and three-body interactions is written in this basis as

$$H = \sum_{ij} H^{(1)}_{ij} c^\dagger_i c_j + \sum_{ijkl} H^{(2)}_{ijkl} c^\dagger_i c^\dagger_j c_l c_k + \sum_{ijklmn} H^{(3)}_{ijklmn} c^\dagger_i c^\dagger_j c^\dagger_k c_n c_m c_l \,, \tag{3.3.2}$$

where the matrix elements for the parts of the Hamiltonian with single-body, two-body and three-body operators are defined as

$$\begin{aligned} &H^{(1)}_{ij} = \langle i|H^{(1)}|j\rangle \,, \quad H^{(2)}_{ijkl} = \langle i,j|H^{(2)}|k,l\rangle \,, \text{ and} \\ &H^{(3)}_{ijklmn} = \langle i,j,k|H^{(3)}|l,m,n\rangle \,. \end{aligned} \tag{3.3.3}$$

Once these matrix elements have been calculated, the matrix elements of the whole Hamiltonian between occupation number states, which form the many-body basis for the Landau level, can be constructed with little effort.

In most of our calculations the total angular momentum is conserved, so that the number of single-particle states is finite, and thus the Landau level projected Hilbert space is

finite. Otherwise, or if the remaining basis is too large, the single-particle basis is suitably truncated by limiting the maximum single-particle angular momentum. The lowest eigensolutions of the largest matrices are obtained by the Lanczos method [68], while the smaller matrices can be completely diagonalized by a standard routine.

3.4 Adiabatic phase factors and time evolution

Berry's adiabatic phase, also called geometric phase, is the remnant of the phase acquired by an isolated quantum eigenstate under cyclic adiabatic time evolution of the Hamiltonian as the dynamical phase factor is factored out. Adiabatic and cyclic time evolution means that the Hamiltonian changes in time infinitely slowly, and that it depends on a set of time-dependent parameters $\mathbf{R}(t)$ that traverse around a loop C in the parameter space and return to their initial value at time T. The eigenstate is assumed isolated, such that its energy does not cross the rest of the spectrum during the cycle. By the adiabatic theorem, the only possible change in the state is a U(1) phase factor

$$|\Psi(T)\rangle = e^{-i\int_0^T \mathrm{d}t E(t)} e^{i\gamma} |\Psi(0)\rangle \,, \tag{3.4.1}$$

where $\hbar = 1$. For N degenerate states, there is correspondingly U(N) transformation in the degenerate subspace, also called Wilczek-Zee phase.

For a well written standard derivation of the explicit values of these phases see Chruściński and Jamiołkowski [69], or the original papers [70, 71, 72, 73]. We merely quote the results. In the nondegerate case, Berry's phase is written as

$$\gamma = \oint_C A = i \oint_C \langle \Psi | d | \Psi \rangle = i \int_0^T \mathrm{d}t \langle \Psi(\mathbf{R}(t)) | \frac{d}{dt} | \Psi(\mathbf{R}(t)) \rangle \,, \tag{3.4.2}$$

where the first two formulas are in the differential form notation. Here A is called Berry's potential one-form, and under phase transformation $|\Psi\rangle \mapsto e^{i\alpha(\mathbf{R})}|\Psi\rangle$, it transforms as $A \mapsto A - d\alpha$, just the same way as the vector potential in electrodynamics. The Wilczek-Zee phase factor $\gamma \in$ U(N) is rather written as a path ordered exponential

$$e^{i\gamma} = \mathcal{P} \exp\left(i \oint_C A \right) \,, \tag{3.4.3}$$

with Wilczek-Zee potential $A_{ab} = i\langle \Psi_b | d | \Psi_a \rangle$, where the indices label the degenerate states in a given basis. Tserkovnyak et al. [74] have numerically evaluated the $\gamma \in$ U(2)

corresponding to adiabatic interchange of quasiparticles for the Moore-Read trial wave function on sphere with four quasiholes by Monte Carlo integration with up to 32 electrons, and they found results in agreement with the effective theory of the Moore-Read phase. Such a direct verification of the non-Abelian statistics is beyond the capability of our approach mainly because of the small electron numbers. In fact, even trapping a single Moore-Read quasihole at the center of a droplet in the ground-state is far from trivial. Wan et al. [65] have succeeded in doing this with about 12 electrons and a gaussian long-range trapping potential. With smaller electron numbers, we tend to get a ground-state with double quasihole, which is a Laughlin-type quasihole. Localizing 4 or even 2 or 1 quasiholes at different positions away from the origin seems to be difficult, as breaking the rotational invariance means we need to content to maximum of about 6 electrons. In any case, the small distance between the quasiholes would break the degeneracy and thus the adiabatic non-Abelianity, though, if the degeneracy is only slightly broken, a non-adiabatic but still much slower than the time scale corresponding to characteristic energy for higher excitations ought to reveal the non-Abelian properties.

To obtain a formula for the following numerics, consider a Hamiltonian parameterized by the location η of a single quasiparticle, that is by the location of the localization potential that is assumed to trap the quasiparticle. The Berry phase in the ground-state, when the quasiparticle traverses around a loop C, is

$$\gamma = i \oint_C \mathrm{d}\eta \langle \Psi(\eta) | \frac{d}{d\eta} | \Psi(\eta) \rangle \,. \tag{3.4.4}$$

It is convenient to set C to be the circle defined by $|\eta| e^{i\theta}$ with $|\eta|$ held constant and $\theta \in [0, 2\pi]$. By symmetry, the state of a quasiparticle located at angle θ is obtained from the state of quasiparticle at $\eta = 0$ by applying the generator of rotations. Then, with unknown 2π periodic phase factor $\varphi(\theta)$

$$|\Psi(\theta)\rangle = e^{i\varphi(\theta)} e^{i\theta M} |\Psi(0)\rangle \,. \tag{3.4.5}$$

Substitution to the formula (3.4.4) for the Berry's base yields

$$\begin{aligned} \gamma &= i \int_0^{2\pi} \mathrm{d}\theta \langle \Psi(\theta) | \frac{d}{d\theta} | \Psi(\theta) \rangle = - \int_0^{2\pi} \mathrm{d}\theta \langle \Psi(\theta) | M + \varphi'(\theta) | \Psi(\theta) \rangle \\ &= - \int_0^{2\pi} \mathrm{d}\theta (\langle M \rangle + \varphi'(\theta)) = -2\pi \langle M \rangle \,. \end{aligned} \tag{3.4.6}$$

Comparing this to the corresponding Aharonov-Bohm phase as explained in the introduction, the charge and statistics of the quasiparticles may be approximated.

Finally, consider other than circular trajectories of quasiparticles and general time evolution. The time-dependent Schrödinger equation has the formal solution

$$|\Psi(t_f)\rangle = \mathcal{T} \exp\left(-i \int_{t_i}^{t_f} \mathrm{d}t H(t)\right) |\Psi(t_i)\rangle \,, \tag{3.4.7}$$

where $\mathcal{T}$ is the time-ordering operator, which orders operators with later time arguments to the left. To numerically compute the time evolution of a given state, we approximate the operator exponential by

$$\mathcal{T} \exp\left(-i \int_{t_i}^{t_f} \mathrm{d}t H(t)\right) \approx \mathcal{T} \prod_{i=1}^{n} \exp\left(-i \Delta t H\left(\frac{t_{i-1}+t_i}{2}\right)\right) \,, \tag{3.4.8}$$

where $t_i - t_{i-1} = \Delta t = \frac{t_f - t_i}{n}$, $t_0 = t_i$, and $t_n = t_f$. We resort to the Krylov space methods, to compute the matrix exponentials as reviewed in [75] and citations therein. In short, with the Lanczos algorithm, the large hermitian sparse matrix exponential is mapped to a smaller real tridiagonal matrix exponential in the Krylov subspace. We then map the resultant vector back to the original truncated Hilbert space. The adjustable parameters are the number of exponentiations n, the small time interval Δt, and the dimension d of the Krylov subspace. Sufficient value of d depends on the size of H and does not significantly affect the computation time for relatively small d. While n is dictated by the amount of time available for our computation, Δt has to be chosen large enough to have approximately adiabatic time evolution, yet small enough to avoid the accumulation of error in the exponentials. Although, the method works and gives the same results for the circular orbits as the previous formula, the continuos reconstruction of the time-dependent part of the Hamiltonian takes fair amount of time, which heavily limits the size of the Hilbert space. In the included results, we thus use only the first method and content to circular orbits.

Chapter 4

Computations

Computations are divided into three main parts. In the first part, we inspect ground-state phase diagrams of the model quantum dot described in Section 3.1. The second part is devoted to the Laughlin filling fractions where the Bose condensation of charge-flux composites, as explained in Chapter 2, is the driving mechanism. The final part studies the paired Moore-Read state associated with the filling fractions $\frac{1}{2}$ and $\frac{5}{2}$, the latter of which corresponds to the half-filled second Landau level with the lowest Landau levels of both spin types completely filled and inert. In the two latter parts, the analysis starts with the identification of the ground-state by computing overlaps with the corresponding trial wave functions and analyzing the conditional wave functions. Then, we proceed with the investigation of the elementary excitations, namely the edge excitations and quasiparticles. Analysis concerning the finite-thickness of the electron layer and possible screening caused by nearby metals is carried out alongside.

4.1 Ground-states of a parabolic quantum dot at a high magnetic field

As will be seen momentarily, the simple two-dimensional quantum dot described by the model (3.1.1) has a remarkable set of diverse ground-states. In what follows, our assumptions are that $\omega_c \gg \omega_0$ and low temperature, so that we can perform a Landau level projection on the nth Landau level as described in Section 3.2. From the single-particle spectrum of the model in Equation (3.1.3), we see that for a fixed total angular momentum M and N electrons, the energy of the ground-state is given by

$$E = N(2n+1)\hbar\omega + M\hbar(\omega - \frac{\omega_c}{2}) + \frac{l}{a_*}\Omega(M,N,n)\,, \tag{4.1.1}$$

where $\Omega(M,N,n)$ is the interaction energy that depends on the form of the interaction, total angular momentum, the number of electrons, and the Landau level index. This allows us to obtain the ground-state angular momentum as a function of the confinement and the magnetic field by diagonalizing the interaction for a range of M with fixed pair (N,n). Contours of the total ground-state angular momentum as a function (ω_0,ω_c) for $(N,n) = (7,0)$ are shown in Figure 4.1. In the phase diagram, there is a particularly vast phase at $M = 63$ corresponding to the Laughlin state at filling $\frac{1}{3}$ as is seen below. The maximum angular momentum is limited to $M = 105$, which is the angular momentum for the next Laughlin state at $\frac{1}{5}$. The opposite limit is the minimum angular momentum of the maximum density droplet, which in this case corresponds to the integer quantum Hall state at $\nu = 1$. As varying ω_0 obviously brings nothing qualitatively new, it is fixed to a reasonable value $\hbar\omega_0 = 2$ meV in the remainder of this section, and the ground-states at different magnetic fields are investigated .

The angular momenta for $(N,n) = (6,0)$ and $(7,0)$ are shown in Figure 4.2. In the first diagram, a very thin phase follows after $M = 39$ at $M = 40$, and the limiting cut for maximum angular momentum $M = 75$ again corresponds to fraction $\frac{1}{5}$. The monotonic trend has a natural explanation in terms of the basis states (Equation 3.1.2). The exponential factor in each single-particle basis state squeezes the state with increasing magnetic field. Therefore, to reduce the Coulomb interaction, the density spreading angular momentum tends to increase, despite the punishment due to confinement potential. For $N < 6$ (figure not shown), the angular momentum is simply quantized to plateaus separated by $\Delta M = N$, starting from the minimum angular momentum $M = \frac{N(N-1)}{2}$.

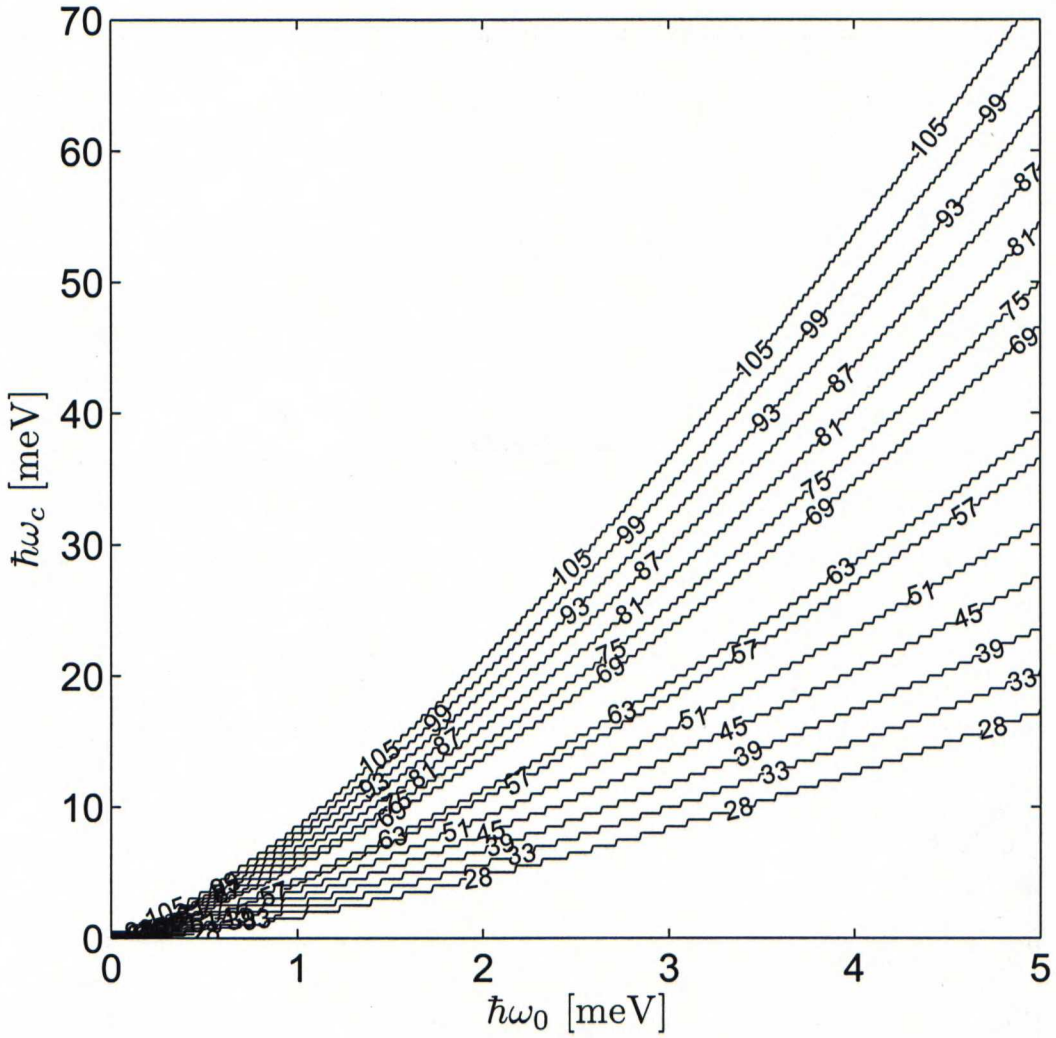

Figure 4.1: Ground-state angular momentum phase diagram for 7 electrons on the LLL interacting through pure Coulomb interaction. Below contour 28, the angular momentum is at the MDD value 21. Maximum angular momentum is limited to 105 by the basis size.

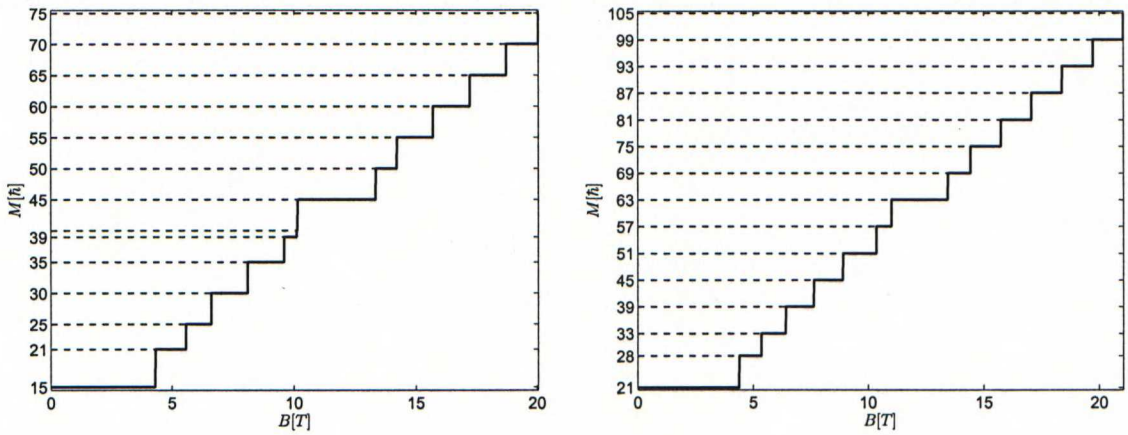

(a) (b)

Figure 4.2: Angular momentum M on the LLL as a function of magnetic field B for (a) 6 and (b) 7 electrons.

For $N = 6$ and 7, there seems to be an additional series of angular momenta separated by $\Delta M = 5$ and 6. The two series admit the following geometric explanation [76, 77].

Consider the ground-state wave function $\psi(z_1, z_2, \ldots, z_N)$ and with electrons placed to the apexes of a regular polygon, $z_i = R\exp(2\pi i/N)$. Such configurations are likely to have a large probability if the size of the droplet is small. Application of rotation $\exp(2\pi i\hat{M}/N)$, where $\hat{M}$ is the total angular momentum operator and the fermi statistics yields $(\exp(2\pi iM/N) + (-1)^N)\psi(z_1, z_2, \ldots, z_N) = 0$. To have non-vanishing wave function for the regular polygonal configuration, we need

$$M = \begin{cases} N(j + \frac{1}{2}), & \text{for } N \text{ even}, \\ Nj, & \text{for } N \text{ odd}. \end{cases} \tag{4.1.2}$$

for integer j. For a larger droplet, we expect high weight for configurations where one electron is placed at the center and the rest are again at the apexes. Calculation now gives

$$M = \begin{cases} (N-1)j, & \text{for } N \text{ even}, \\ (N-1)(j + \frac{1}{2}), & \text{for } N \text{ odd}. \end{cases} \tag{4.1.3}$$

The pair correlation functions and densities of the droplet confirm the above assertions about the preferred configurations [77]: The states in both series have strong pair correlations for the suggested configurations and show a peak in the density profile at a certain distance away from the origin. In addition, the states in the $N-1$-series have another density peak at the center of the droplet.

Alternatively, the magic angular momenta can be explained by the mean-field composite-fermion theory in terms of compactly filled Landau levels of composite-fermions [78]. However, at high enough angular momenta the mean-field model is inaccurate but as shown recently [79], taking into account the interaction between the composite-fermions improves the predictions.

The angular momentum of the Laughlin state at filling fraction $\frac{1}{2m+1}$ in the presence of q_h quasiholes and q_e quasielectrons is (see Section 1.1.3)

$$M_{m,q_h,q_e} = \frac{(2m+1)N(N-1)}{2} + (q_h - q_e)N \,. \tag{4.1.4}$$

Hence, some of the states in the N-series of angular momenta are supposedly related by quasiparticle excitations. In fact, for $N \leq 5$ they all are, which in part motivated Laughlin (who used only 3 electrons in numerics) to formulate the trial wave functions for quasiparticles. On the contrary, for $N = 6$ and 7 the Laughlin's quasihole over $\frac{1}{3}$ is not a preferred ground-state unless a disturbation is introduced to to push charge away from the center. It is easy to check that the Laughlin state with $q_e = q_h = 0$ belongs to both N and $N-1$-series for all N, so the density has a double-peak structure for $N \geq 6$ but only a single peak at the center for $N \leq 5$.

The ground-states of quantum dots at higher Landau levels are less well explored in the literature. We have found that also on the SLL for $N < 6$, $M(B)$ is a stair-case with characteristic step height N (figure not shown). As seen in Figure 4.3a, for $N = 6$ the by now familiar $N-1$ stair case emerges but, in addition, there are two ground-states at $M = 25$ and $M = 31$, which do not fit in the preceeding discussion, the first of which at least has a good overlap with one of the edge excitations in the $\Delta M = 4$ sector of the Moore-Read quantum Hall state. Interestingly, the angular momentum of $\nu = 2 + \frac{1}{2}$ Moore-Read state[†], $M = 21$, is realized as a ground-state on the SLL, while it was not on the LLL. In addition, the angular momentum $M = 39$ corresponding to the $\nu = 2 + \frac{1}{3}$ Laughlin state is clearly less stable than $\nu = \frac{1}{3}$ on the LLL. This is consistent with the softening of the interaction at short distances in the higher Landau levels as indicated by the Haldane pseudopotential parameters that show decreasing resemblance to the exact model interaction with increasing Landau level. For $N = 7$ and 8, there is similarly additional states, so the ground-states differ in general from the LLL phases.

[†]Moore-Read state at a higher Landau level is obtained by applying the Landau level raising operator to each electron n times in the Moore-Read wave function. In terms of the basis states, the mapping is $|0, l\rangle \mapsto |n, l-n\rangle$ so that the angular momenta are $M_{n\text{LL}} = M_{\text{LLL}} - nN$.

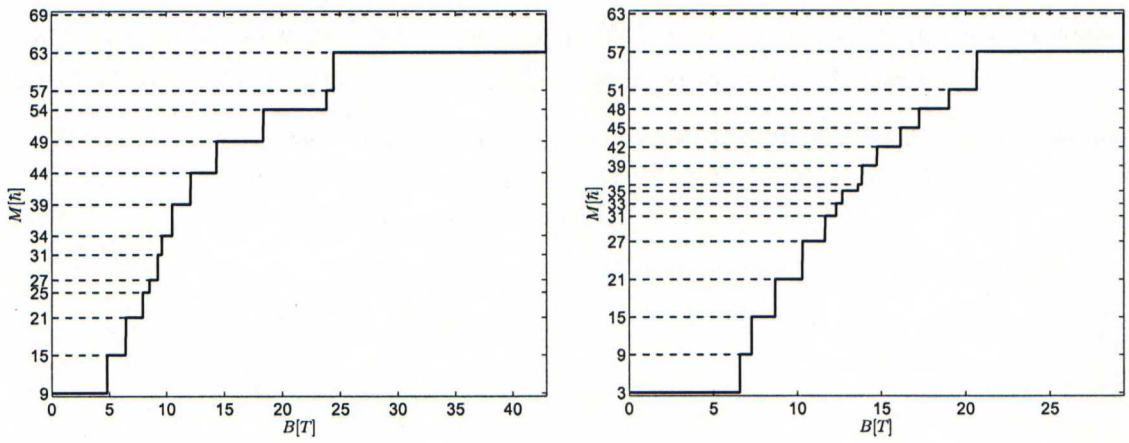

(a) (b)

Figure 4.3: Angular momentum M on (a) the SLL and (b) the TLL as a function of magnetic field B for 6 electrons.

On the third and higher Landau levels, $M(B)$ has more complicated structure shown in Figure 4.3b for 6 electrons. There is a pattern of phases separated by $\Delta M = N$ for small and large angular momenta. At intermediate values, the separation is $\Delta M = N/2$ with the exceptions $M = 31$ and 35. The $M = 15$ phase corresponding to the angular momentum of Moore-Read state is again supported. Here it is a part of a firm series of phases separated by $\Delta M = N$. This suggests that it could be an integer filling fraction state with 2 quasiholes.

At a low density the elecrons will crystallize and form a Wigner crystal. The geometric derivation of the $N-1$ and N series of angular momenta relies on two plausible crystal structures for a few-electron droplet. The liquid character of the droplet can be increased by taking into account the small thickness of the electron layer. The more liquid-like droplet with finite thickness might then favor the N series associated also with the quantum Hall liquid rather than the $N-1$ series. This is the case in Figure 4.4a for 6 electrons on the LLL where some of the $N-1$ states are no longer present. On the SLL the effect is even stronger, and all the states are separated by angular momentum N as seen in Figure 4.4c. However, too much thickness destroys the vital short-range repulsion necessary for the Laughlin states to form. Screening of the interaction seems to favor the $N-1$ series, and especially the Laughlin state at LLL as seen in the Figures 4.4b and 4.4d.

In conclusion, we have seen that the effective inter-electron interaction has strong influence on the stability of different ground-state phases. Moreover, ground-states corre-

sponding to angular momenta equal to that of the Laughlin states are especially favored in the LLL in the presence of screening. The ground-state angular momenta corresponding to the Pfaffian state are readily found at the higher Landau levels but on the LLL only when the finite-thickness of the wave function in z-direction is taken into account. However, the ground-state angular momenta of course in no way guarantees that the states in question are related to the Laughlin or Pfaffian states. The relation of the realistic states to the theoretical states will be investigated in the following sections.

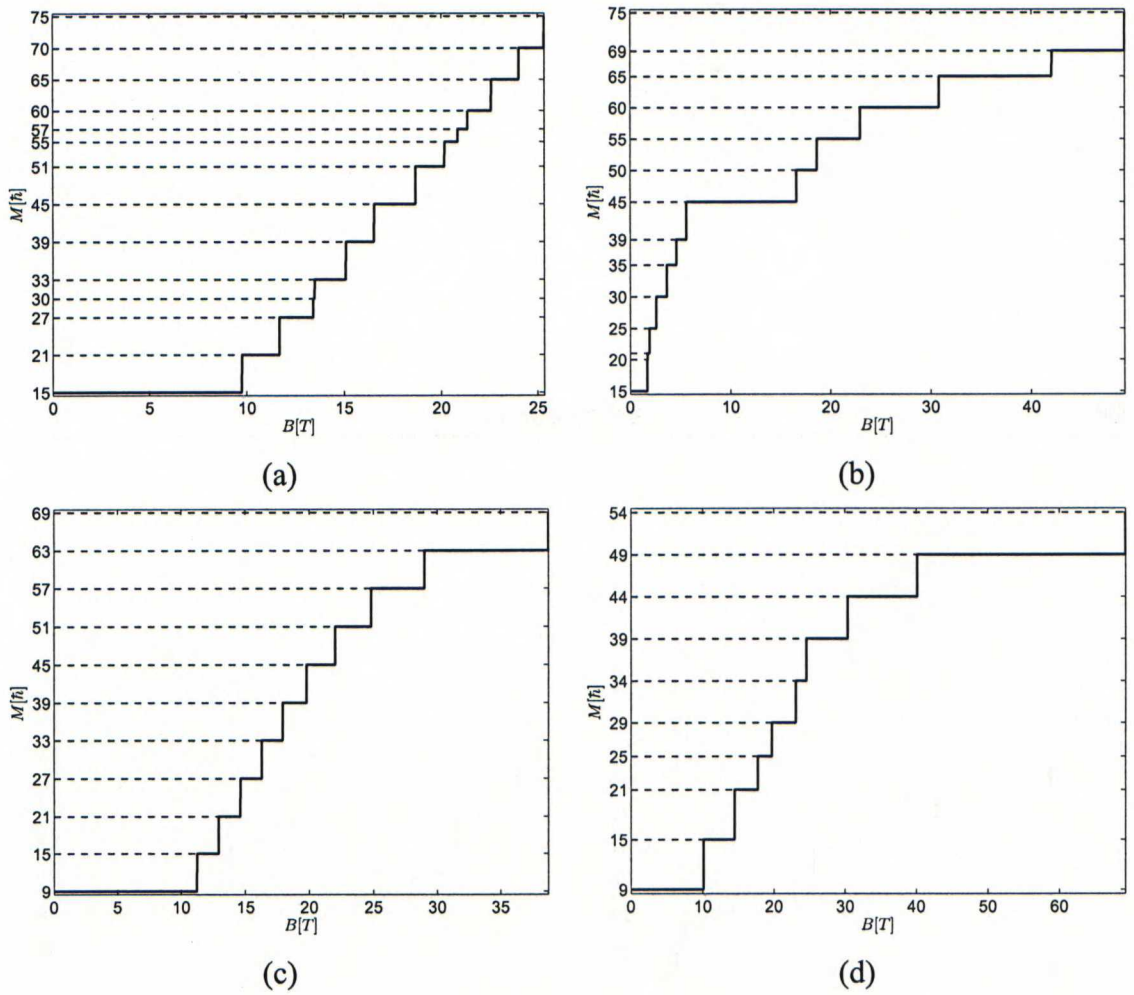

Figure 4.4: Angular momentum M of 6 electrons at different magnetic fields on the LLL with (a) $(d_t, d_s) = (2, 0)$ and (b) $(d_t, d_s) = (0, 1)$ (exceptionally with $\hbar\omega = 0.5$ meV), and on the SLL with (c) $(d_t, d_s) = (2, 0)$ and (d) $(d_t, d_s) = (0, 1)$.

4.2 The primary Laughlin filling fractions

4.2.1 Binding-unbinding transition of charge and flux

At this point, we wish to investigate the binding of flux to electrons, which is the essence of the fractional quantum Hall effect. In particular, the primary filling fractions $\nu = \frac{1}{2m+1}$ submit to explanation in terms of the Bose condensate of charge-flux composites as reviewed in the beginning of Chapter 2. In the numerics, we content with the two first filling fractions in the sequence. As seen momentarily, the flux-binding depends on the screening and finite-thickness incorporated to the interaction.

Let us fix $N-1$ of the electron co-ordinates in an N electron wave function. The remaining function is called the conditional wave function, and it is proportional to an analytic polynomial times an irrelevant exponential factor on the LLL. The conditional wave function gives information about the pattern of zeros of the many-body wave function, most clearly illustrated by its phase, which must change by 2π around each root. Figure 4.5 shows the phase of the conditional wave function for the 3-electron ground-states with angular momenta corresponding to $\frac{1}{3}$ Laughlin state with a quasihole and bare $\frac{1}{5}$ Laughlin state when the interaction is pure Coulomb. The notable difference to the exact Laughlin states is the displacement of the vortex positions along the line of the center of mass of the system and positioning of the additional vortex on this line instead of the origin.

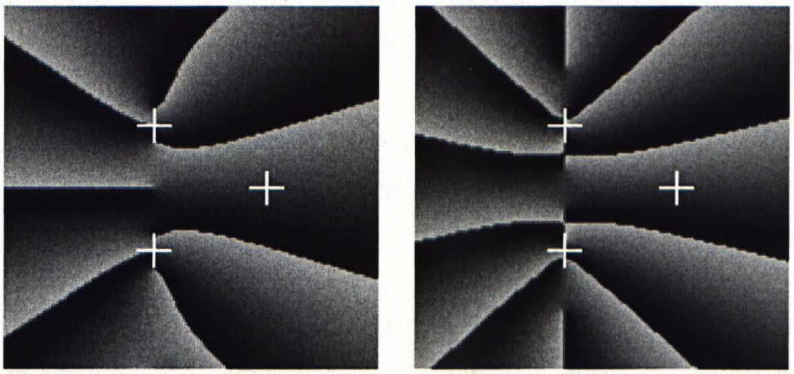

(a) (b)

Figure 4.5: Phase of the conditional wavefunctions of the $\frac{1}{3}$ state with one quasihole, or vortex, and a plain $\frac{1}{5}$ state, both with three electrons.

The binding of flux to the electrons can be quantitatively analyzed by computing the overlap with the exact Laughlin state, in which the zeros, or flux, are precisely bound on top of electron positions. Figure 4.6 shows the overlaps for 3 to 6 particles with the $\nu = \frac{1}{3}$ Laughlin state, when the screening and layer thickness are varied. Remarkably, the overlaps go to unity with the strong screening indicating an exact condensation of zeros to the electron co-ordinates. This is not a surprise, as the Haldane pseudopotential coefficients indicated similarity between screened Coulomb interactions and the exact model interaction. The layer thickness reduces the overlap, which is consistent with the flattening of the corresponding Haldane parameters in Section 3.2. Similarly, on the higher Landau levels, the overlap (with the raised Laughlin state) becomes smaller. Note also that a small thickness, always present in the real system, does not yet destroy the overlap.

The phase of the conditional wave function in Figure 4.7a for strongly screened Coulomb interaction with tightly bound zeros looks exactly like that for the Laughlin state as it should. Similarly, in Figure 4.7b the zeros of the wavefunction have moved far away from the particle positions as the layer thickness is increased. See Figure 4.5 for comparison to the strictly two-dimensional system.

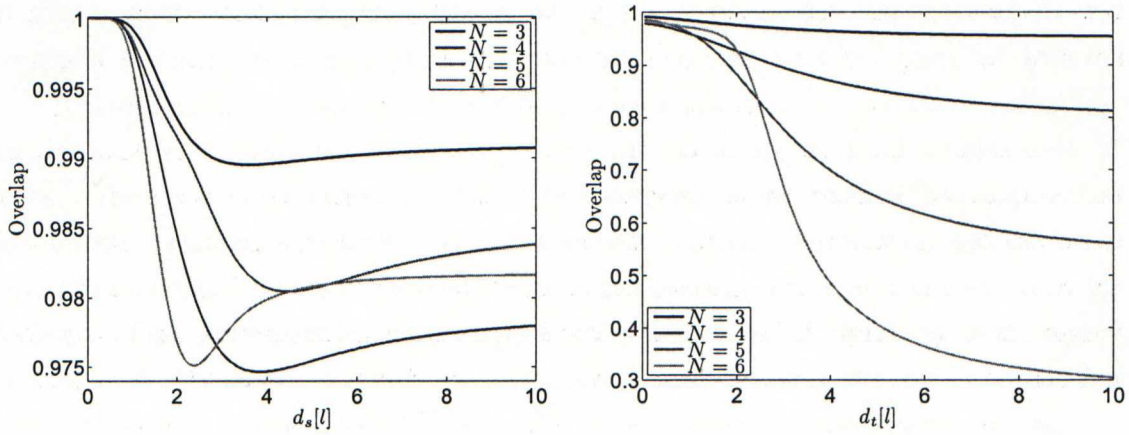

Figure 4.6: Overlaps with the $\frac{1}{3}$ Laughlin state for (a) the screened and (b) the thick-layered Coulomb interaction.

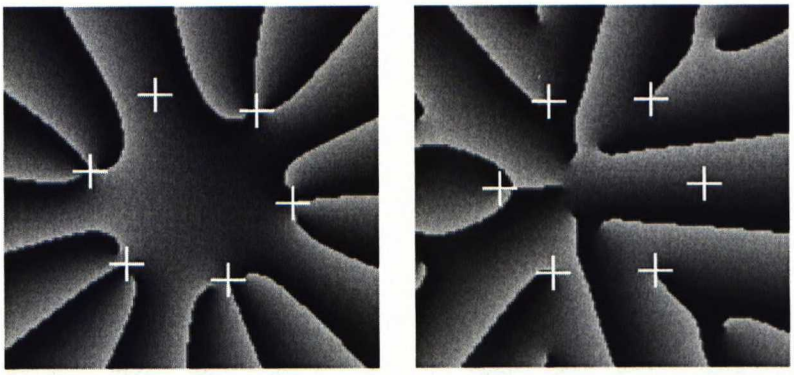

(a) (b)

Figure 4.7: Conditional phase for the (a) screened ($d_s = l$) and (b) thick-layered ($d_t = 5l$) solutions at filling fraction $\frac{1}{3}$ for 6 electrons. The most likely configuration (up to rotation) and fixed co-ordinates are indicated by a plus.

4.2.2 Creating and localizing vortices

To create vortices in a quantum dot, that correspond to the Abelian anyons observed in the quantum Hall effect at $\nu = \frac{1}{3}$, we first set the confinement and magnetic field suitable for a ground-state in the topological phase of the Laughlin state. Typical parameters are $B = 10$ T and $\omega_0 = 2$ meV. For $N \leq 5$, a vortex at the center of mass can now be created by decreasing confinement or increasing magnetic field, and also for $N = 6$ (and plausibly $N \geq 7$) if a small thickness to the electron layer is introduced as was seen in Figure 4.4 (there the stability at angular momentum 45+6 indicates the stability of the quasihole state). Alternatively, a strong enough local repulsive potential will create a charge deficiency in the form of a vortex.

In Figure 4.8a, a single vortex is trapped to the center of the droplet by a gaussian potential (Equation (3.1.7)). As the strength of the gaussian is increased, a second and third vortex join in as seen in Figures 4.8b and c. Recall that if these were ideal Laughlin quasiholes in a macroscopic sample, their charges ought to be $\frac{e}{3}$, $\frac{2e}{3}$ and e, respectively. With three vortices, the perturbation has already caused those zeros that are ideally bound to electrons to displace further, indicating a break-down of the Laughlin state due to too strong localization potential.

We next further investigate the effect of the strength of the localization potential. Angular momentum is fixed to the single Laughlin quasihole state's value and localization

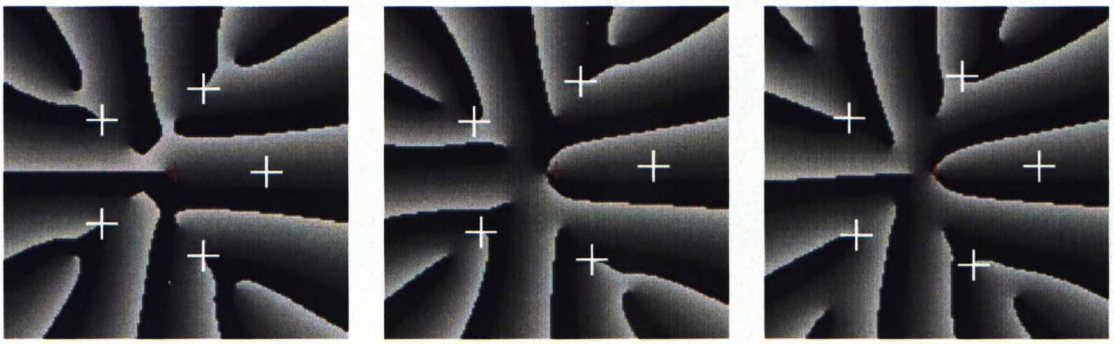

(a) (b) (c)

Figure 4.8: Phase of the conditional wave function for a ground-state with single, double, and triple vortex at the origin induced by $(W, s) = (5, 1), (10, 1)$, and $(20, 1)$, respectively. The red + indicates the disturbance in the middle, and otherwise markers are as in Figure 4.7.

potentials with various ranges are considered. We compute the overlap of the state with the exact Laughlin's quasihole state as a function of the strength of the localization potential W for three and five electrons. The results are shown in Figure 4.9. At $W = 0$, the overlap is small because the vortex is positioned at the center of mass co-ordinate unlike the Laughlin vortex, which is strictly at the origin. As W is increased, the overlap

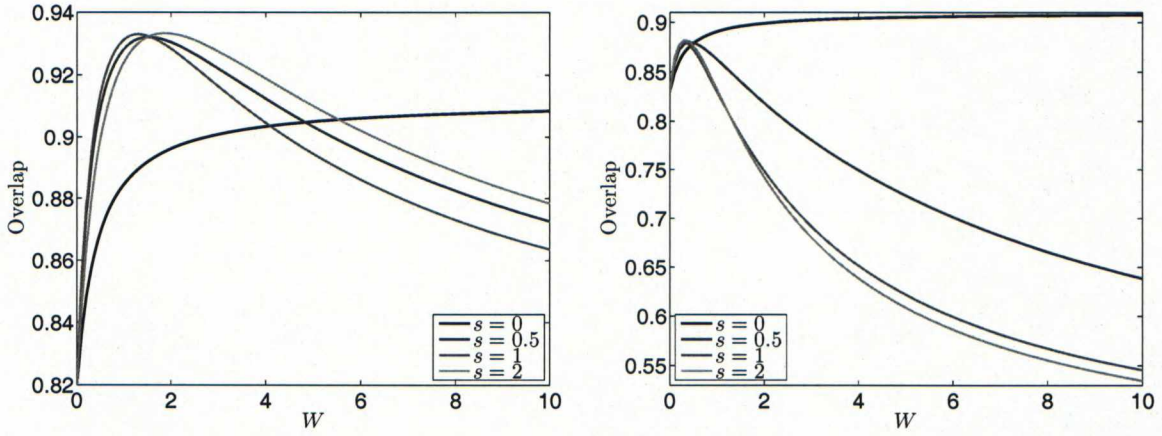

(a) (b)

Figure 4.9: Overlaps of Laughlin quasiholes with vortices trapped with strength W, range s gaussian potentials for $N = 3$ and $N = 5$.

becomes larger as vortex becomes localized to the origin. For the finite range gaussian potentials, the overlap starts to decrease after a critical value as the potential may push too much charge away from its way. The small overlap at large W indicates an unbinding transition in the Laughlin state as was seen in Figure 4.8c for the triple vortex. In contrast, the strictly local delta function potential has a monotonically increasing overlap, this is because effectively only the point 0 is removed from the configuration-space, while the Laughlin's quasihole wave function is 0 at $z_i = 0$ anyway. In general, however, we would like to localize the vortex with as weak potential as possible to least disturb the state and the remnants of topological properties.

Although much more difficult, the vortex can also be trapped away from the center thus breaking the rotational invariance. Figure 4.10 shows the electron densities and the phases of conditional wave functions for the four and six electron systems when the localization potential is at radius 3. Interestingly, the flux seems to be well attached to the electrons while the density distributions show clear localization of electron positions with N separated peaks.

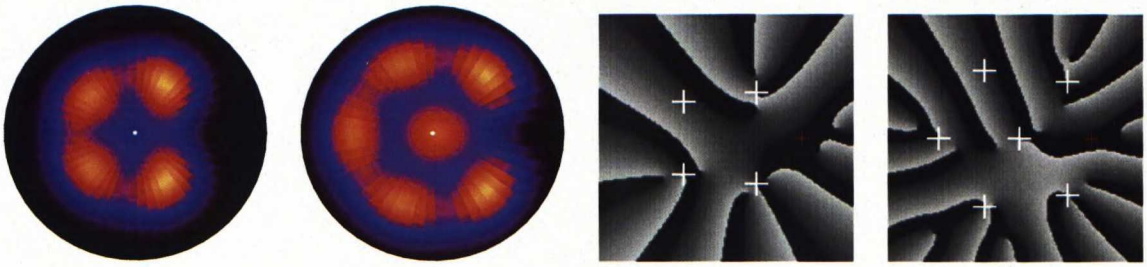

(a) (b) (c) (d)

Figure 4.10: The charge densities and phases of conditional wave functions corresponding to a filling fraction $\frac{1}{3}$ quasihole at radius $|\eta|$ computed by the Berry phase for (a,c) four and (b,d) six electrons, respectively, with parameters $B = 10$ T $\omega_0 = 3$ meV $(W, s) = (3, 2)$ in both.

4.2.3 Density fluctuations and the fractional charge

In the previous subsection, the vortices were created at the center, the electron density taking the form of an annulus. In this case, the charge and size of the vortex can be estimated by subtracting the density without a vortex from the density in the presence of a vortex and integrating from zero to r to obtain the charge deficiency inside radius r. Once the cumulative charge ceases to increase, the edge of the vortex has been reached. Figure 4.11 presents the cumulative charge densities for the $\frac{1}{3}$ Laughlin state and the corresponding state with Coulomb interaction for N electrons. In both cases, the radius of the vortex is of the order of one to two oscillator lengths, and the charge fluctuates around 0.4 times the elementary charge. For the Coulomb interaction, the fluctuations are stronger due to the long-range nature of the interaction. Furthermore, for $N = 6$ and 7 the cumulative charge has a double-peak structure following from the double-peak structure of the ground-state density profiles mentioned in Section 4.1.

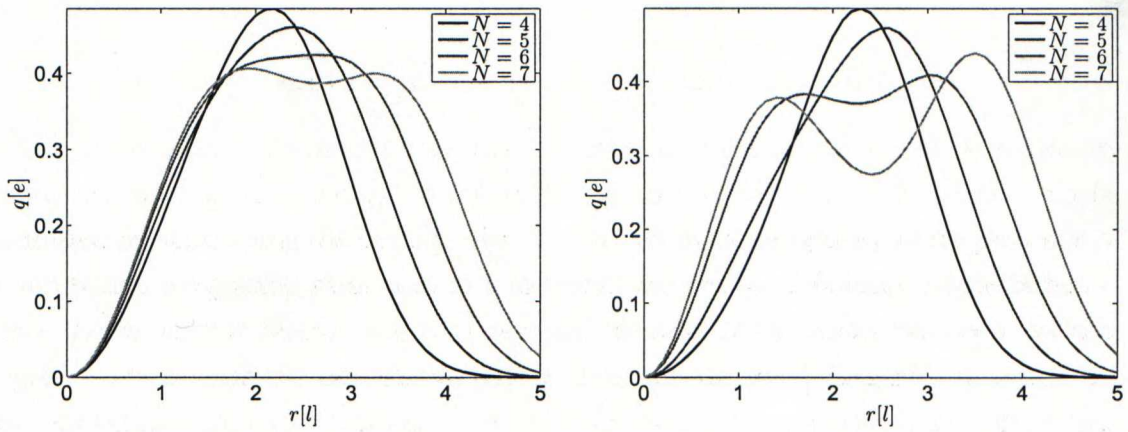

Figure 4.11: Cumulative quasihole charges at filling fraction $\frac{1}{3}$ for (a) the exact model interaction and (b) the Coulomb interaction for a single quasihole at the center.

When the vortex is localized at radius $|\eta|$, the charge can be estimated by the Berry phase as explained in Chapter 3. The charges thus obtained for a vortex at filling $\frac{1}{3}$ are displayed in Figure 4.12 for $N = 4$ and 6. Because of finite-size effects, the charge fluctuates strongly as a function of position. For four electrons, the charge seems to be closest to the $\frac{e}{3}$ between radius 2 and 3, and for six electrons at radius less than 2. These finite-size effects are related to the peak structure of the density since in a small size

density-fluctuating droplet a quasihole is preferredly created near the density peaks, and the maximum in density at 0 for $N = 6$ allows a particularly stable vortex near the center. The absolute value of charge can be slightly shifted by varying the magnetic field and confinement, which reflects the problemacy in determining the charge in a small system by the Berry phase method. The seemingly negative charge for 4 electrons at distances around 1 oscillator length are presumably due to a stronger opposite sign charge fluctuation created opposite to the localization potential.

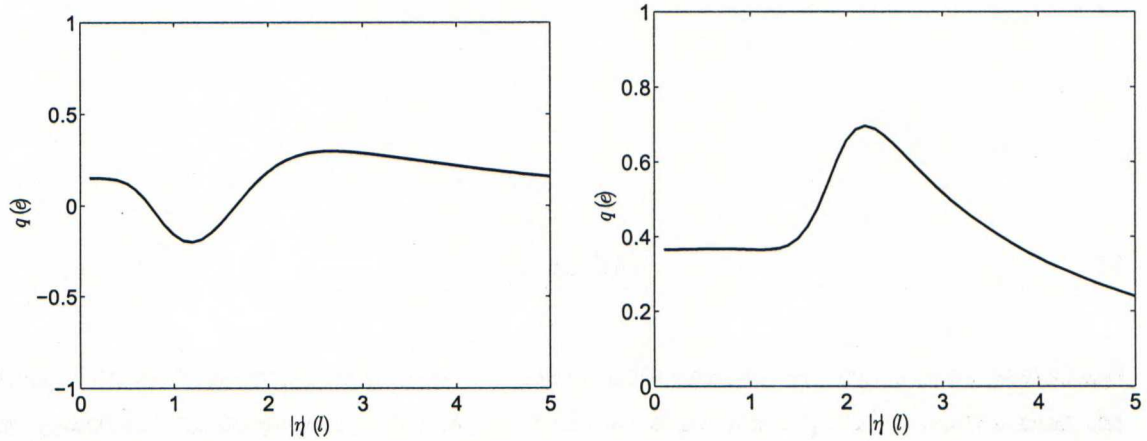

Figure 4.12: The charge of a filling fraction $\frac{1}{3}$ quasihole at radius $|\eta|$ computed by the Berry phase for (a) four and (b) six electrons, respectively, with parameters $B = 10$ T $\omega_0 = 3$ meV $(W, s) = (3, 2)$ in both.

If we settle for vortices above filling fraction $\nu = 1$, the electron number can easily be taken up to 60. Figure 4.13 shows the charge of the vortex obtained with the Berry phase. The charge seems to be constant up to a radius of about $5l$ after which it doubles and starts decreasing. We have verified that after the jump there is actually a localized double vortex with the selected strength of the gaussian potential, which explains the doubling of the charge. However, the charge of a hole is expected to be equal to the elementary charge, so there is a clear deviation that must be due to the perturbation caused by the localization potential, though the result for charge can again be little adjusted by varying the magnetic field and confinement within the allowed range for the phase of ground-state.

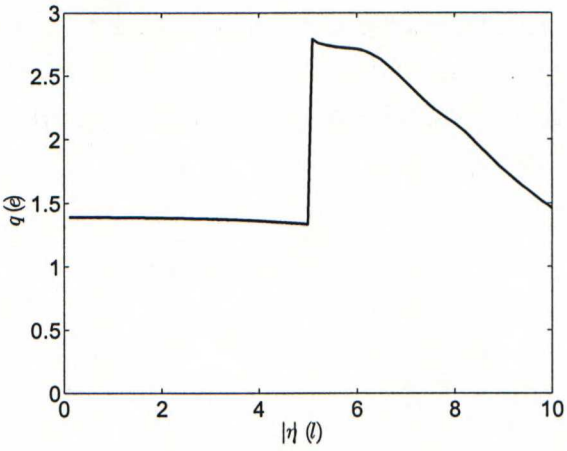

Figure 4.13: The charge of a filling $\nu = 1$ hole at radius $|\eta|$ computed by the Berry phase for 60 electrons, with parameters $B = 5$ T, $\omega_0 = 3$ meV and $(W, s) = (30, 1)$.

4.2.4 Bosonic edge modes

The ground-states that are especially stable (say the universality class of Laughlin state at $\frac{1}{3}$ on the LLL) have typically a special configuration and are thus separated from the rest of the spectrum with the same angular momentum by a large gap in the interaction energy. For larger angular momenta, the interaction energy of course decreases and the ground-state with finite angular momentum is obtained after the confining potential is introduced. As discussed previously, the quantum Hall states in a manifold with a boundary have ideally low-energy edge excitations, which lead to a separate low-energy sector of the spectrum. This is now investigated with realistic interaction potentials. The results shown are computed with 5 electrons but similar results are obtained with other small numbers of electrons.

Figure 4.14a shows the interaction energy spectra on the LLL for angular momenta up to $M = 53$ for the model interaction (Equation (3.2.6)). The angular momenta for $\frac{1}{3}$ and $\frac{1}{5}$ Laughlin states are 30 and 50. The sequence of zero-energy states starts from the non-degenerate state at $M = 30$ and is separated from the rest of the spectrum by a clear gap. For convenience, we call the low-energy part of the spectrum the edge spectrum as it can be considered the set of edge excitations of the $\frac{1}{3}$ state. The state with $M = 50$ corresponding $\nu = \frac{1}{5}$ is then an edge excitation obtained by multiplying with the symmetric polynomial $\prod_{i<j}(z_i - z_j)^2$. However, in practice the edge excitations with

large angular momentum difference to the ground-state acquire a colossal gap once the confinement of the quantum dot is introduced. In a macroscopic quantum Hall sample, the confinement may be smoother but the number of electrons is correspondingly larger (so that ΔM is larger) so that the $\frac{1}{5}$ Laughlin state is in practice of course not a low-energy excitation of $\frac{1}{3}$ Laughlin state. Generally speaking, this means that as far as the physical state in the quantum dot at a low temperature is considered (or alternatively the thermodynamic limit of macroscopic quantum Hall sample is roughly approximated), only few first of the edge excitations following a given state are relevant to the ground-state properties of the phase of that state.

To come back to the energy spectrum in Figure 4.14a, we have counted that the degeneracies of the zero energy states of the $\frac{1}{3}$ state agree with those obtained in Section 2.1. For five electrons, the number of modes compared to the thermodynamic limit are repeated in Table 4.1 The low-energy spectrum of the model interaction in the thermodynamic limit is interpreted as a branch of bosonic edge modes. The fact that the model potential is obtained in the limit of short screening length implies that these results also hold for a sufficiently screened Coulomb interaction.

Table 4.1: Number of edge states of the Laughlin states with angular momentum ΔM for five electrons and at the thermodynamic limit.

ΔM	0	1	2	3	4	5	6	7	8	N
	1	1	2	3	5	7	10	13	18	5
	1	1	2	3	5	7	11	15	22	∞

The corresponding energy spectrum for an unscreened Coulomb interaction is shown in Figure 4.14b. Clearly there is a significant gap at the first Laughlin state at $M = 30$ and a smaller gap at the second Laughlin state at $M = 50$. The well gapped states at $M = 25$ and 35 presumably correspond to the quasielectron and quasihole states. Unlike with the previous model interaction, there is no such clear distinction between the edge spectrum and bulk excitations. However, there seems to be a few gapped states right after $M = 30$, on which we now take a closer look.

The low-lying states, all of which are non-degenerate, are shown in Figure 4.15a. The state at $M = 31$ and the two states at $M = 32$ are well separated from the higher spectrum and are readily interpreted as edge excitations and have the correct count. Moreover, since the angular momentum raising operator, which can be used to generate edge excitations,

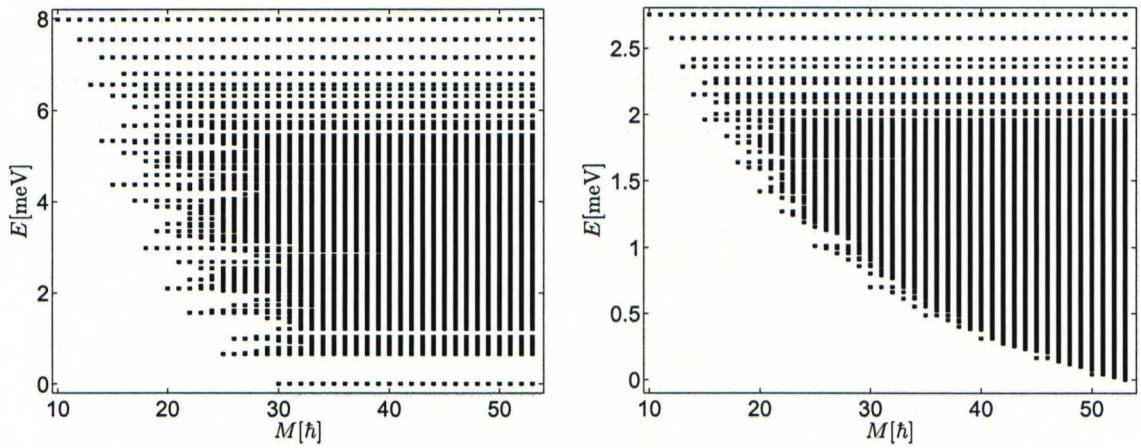

(a) (b)

Figure 4.14: LLL interaction energy spectra for angular momenta up to angular momentum of $\nu = \frac{1}{5}$ for (a) the ideal short-range and (b) the Coulomb interaction with 5 electrons. There is no natural energy scale for the left figure so the scale is arbitrary.

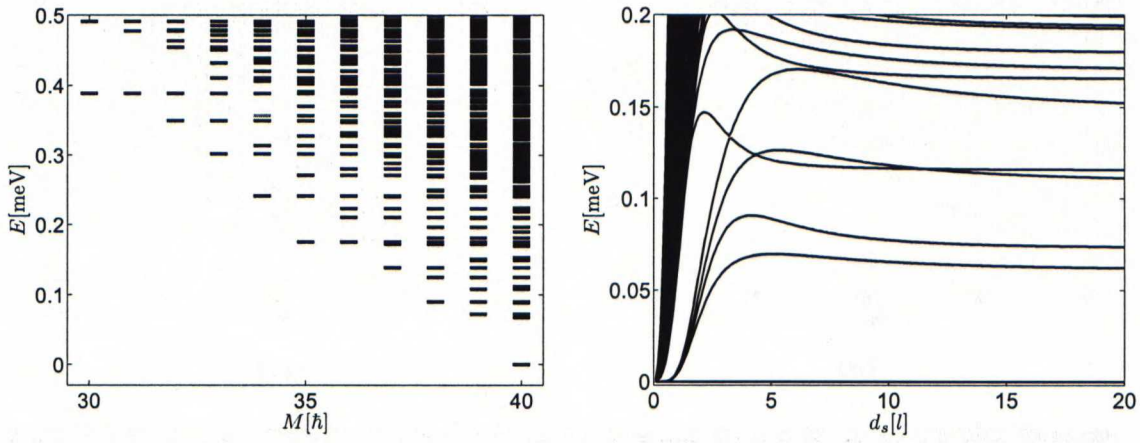

(a) (b)

Figure 4.15: (a) The low-lying states of Figure 4.14b starting from the first Laughlin state at $M = 30$ and (b) the low-energy spectrum for $M = 34$ as the screening is varied.

commutes with the interaction potential, an energy state at M implies energy state at $M + 1$ at the same energy. We anticipate the lowest energy state to be part of the edge spectrum and that the interaction energies do not increase as M goes higher. Therefore, we are confident that the three states at $M = 33$ also correspond to edge excitations, although there no longer is a gap. However, at $M = 34$ there seems to be exactly one bulk state mixed with the low-lying states. To resolve the discrepancy, the lower part of the spectrum with $M = 34$ is plotted as a function of the screening, with the lowest energy shifted to $E = 0$ in Figure 4.15b. Recall that at small screening length the spectrum becomes the ideal spectrum considered above, so the two bands starting from small d_s correspond to the bulk and edge excitations. The bulk excitation that first separates from the bulk band is mixed with the edge excitations and forms the fifth state at $d_s \to \infty$. The bulk state is indicated by the gray bar in Figure 4.15. At higher M, the mixing is more severe, although the bulk and edge excitations can in principle be distinguished as above. The situation is improved by introducing screening. As seen in Figure, 4.15b, a screening with $d_s \approx 3l$ removes the mixing at $M = 34$. The thickness tends to have an opposite effect and reduces the gaps. This is consistent with the previously discussed binding-unbinding transition.

Finally, we consider the interaction energy in the presence of a strong short-range repulsive potential at the center. As seen in Figure 4.16, the spectrum separates into two parts. There is one state at the minimum angular momentum of the maximum density droplet $M = 10$, which is the integer Hall state corresponding to $\nu = 1$ ($\Psi \propto \prod(z_i - z_j)$). All the rest of the states can be obtained from it by a multiplication with a symmetric polynomial. The low-energy spectrum starts at $M = 15$, which corresponds to a hole excitation of $\nu = 1$. Its edge excitations, that is the whole low-energy sector of the spectrum, can similarly be obtained by a multiplication of the hole wave function with a symmetric polynomial. Hence, the number of states in the low-energy spectrum at each $M = 15 + \Delta M$ is precisely given by the partitions presented in Section 2.1.

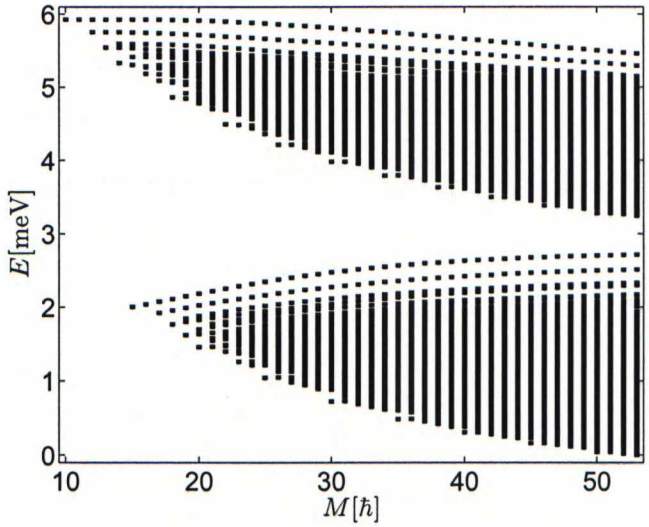

Figure 4.16: The spectrum for 5 electron droplet with a delta function puncture of strength $W = 10$ in the origin.

4.3 Half-filled first and second Landau level

4.3.1 Towards the Moore-Read state in a quantum dot

In Section 4.1, it was seen that with the Coulomb interaction ($d_t = d_s = 0$) the ground-state at the angular momentum of the Moore-Read, or the Pfaffian, state for 6 electrons $M = 27 - Nn$ was supported only at the SLL and TLL. Moreover, it was also supported on the LLL when a finite-thickness of the electron layer was present in the effective interaction. In what follows, we investigate with a few different electron numbers what is the relation between the state obtained with a realistic interaction and the Moore-Read state. This is done by comparing the overlaps of the solution state with the Moore-Read trial wave function, and additionally, by investigating the phase structure of the wave functions and the low-energy excitations.

Figure 4.17a shows the overlaps as a function of the electron number on the three lowest Landau levels with the Coulomb interaction. With four particles, the overlap on the TLL is near the unity, however, increasing particle number rapidly decreases the overlap clearly below the corresponding overlaps at the lower Landau levels. On the contrary, on the SLL the overlap remains reasonable at higher electron numbers, while the LLL overlaps are placed in between these two. Therefore, we content ourselves to the two lowest Landau levels in the reminder of this part.

Figure 4.17b, c, and d show the overlaps on the two lowest Landau levels at different screening and thickness parameters for electron numbers $N = 4$, 6 and 8, respectively. Note that the overlaps at $d_s \to \infty$ and at $d_t = 0$ should be equal. With four electrons, the overlap on the LLL increases steadily when the thickness is increased, though this finite-size artifact is lost at higher electron numbers. Still, at six and eight electrons there is a peak at the preferred thickness near $d_t = 2$ with a very high overlap. These are also realized as the ground-state as seen in Section 4.1. Screening the interaction decreases the overlap on the LLL. On the SLL the situation is opposite, as the thickness has a negative effect for all considered electron numbers but screening favors the Moore-Read state. Recalling that screening pushes the effective interaction towards lower Landau level and thickness towards higher Landau levels, this means that in few-electron quantum dots, the Moore-Read state is especially favored when the effective interaction is between that of the LLL and SLL. Still the overlaps are not high enough for drawing a conclusion that in the thermodynamic limit the Pfaffian state possesses the same topological properties as

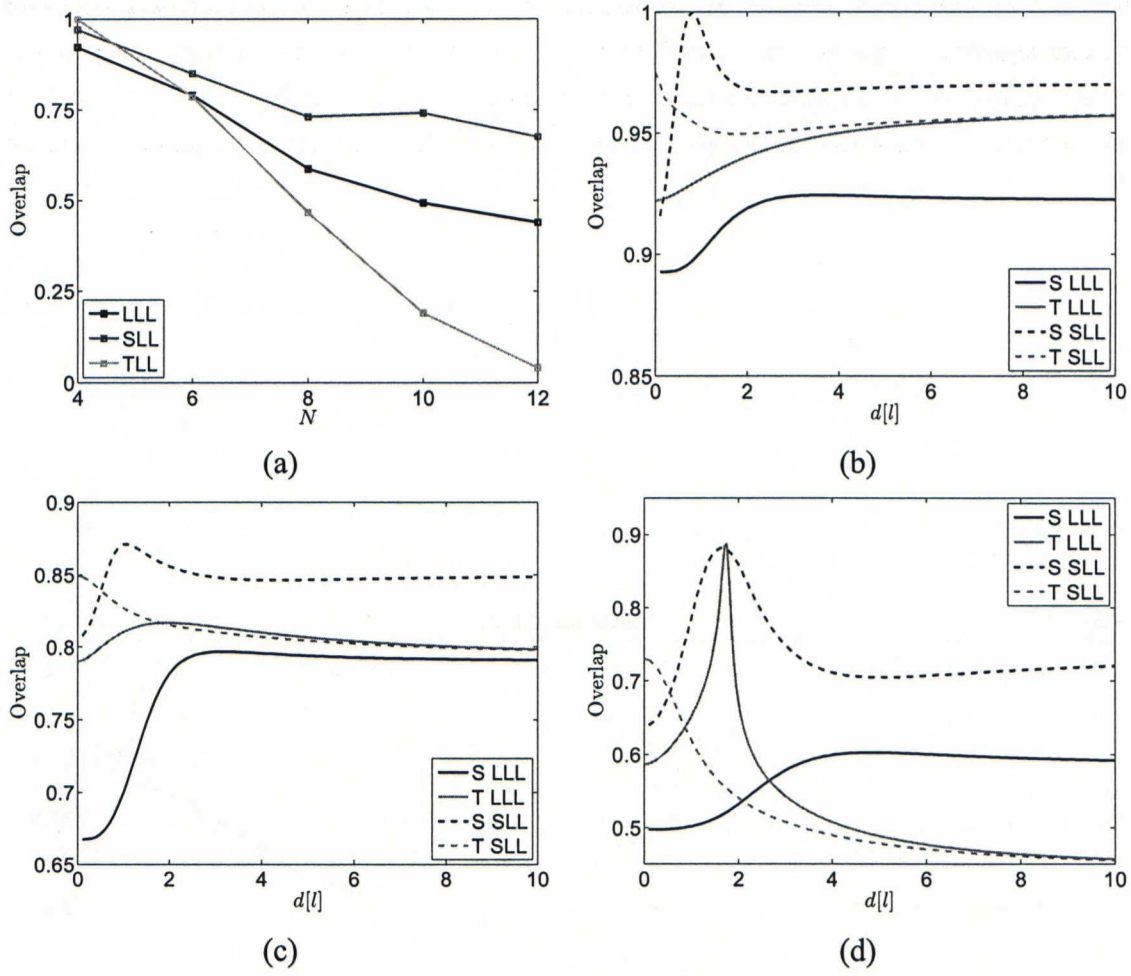

Figure 4.17: Overlaps on the three lowest Landau levels with the pure Coulomb interaction (a) for even electron numbers N and overlaps on the lowest and second lowest Landau levels as a function of screening (S) and thickness (T) parameter for $N = 4, 6, 8$ in figures at (b), (c), and (d), respectively.

the realistic counterpart.

The conditional wave functions can also be instructive. Figure 4.18 presents the phases of the conditional wave functions for $N = 6$ and 8 for the Moore-Read state and the state with Coulomb interaction on the two lowest Landau levels, where the electron coordinates are optimized to the preferred configuration that maximizes the wave amplitude. On the SLL, the wave function is mapped to the LLL by using the Landau level lowering operators in order to have better a comparison. With 6 elecrons, all the phase diagrams

and electron configurations look quite similar, which is understandable in the light of the high overlaps in Figure 4.17a. On the contrary, for eight electrons the overlap on the LLL clearly drops, as the configuration with two electrons at the center becomes favorable. Physically, this leads to a peak in the electron density at the center, and a repulsive local potential can be used to increase the overlap and restore a ring-like configuration. On the SLL this does not happen and the overlap remains better.

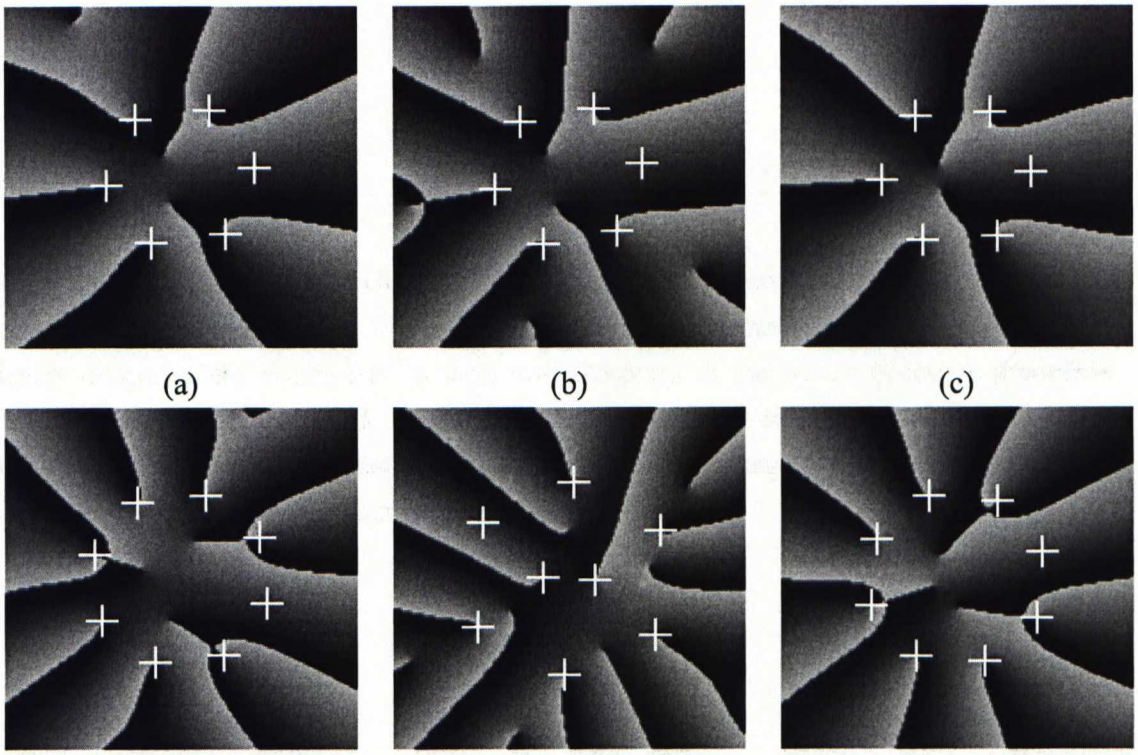

Figure 4.18: Phase of the conditional wave functions with $N = 6, 8$ for (a,d) the Pfaffian states and the corresponding states on the (b,e) LLL and (c,f) SLL with pure Coulomb interaction. The most probable configuration of electrons is marked by a plus.

4.3.2 Excitation spectra and edge modes

In the previous part, as we investigated the primary Laughlin filling fractions, we found the bosonic branch of edge excitations with the model potential (Equation 3.2.6) and the mixing of the edge excitations to the bulk spectrum for realistic potentials. This time, we expect to find a combination of bosonic and fermionic edge modes as explained in Section 2.2. The spectrum is obtained by diagonalizing the exact model potential (Equation 3.2.7), which gives the Moore-Read state as the lowest angular momentum zero-energy eigenstate, and is then compared to spectra obtained with the effective Coulomb interactions.

Figure 4.19a shows the spectrum of the model three-body interaction for 6 electrons up to total angular momentum $M = 43$. The lowest angular momentum zero-energy state at $M = 27$ corresponds to the Moore-Read state, and it is followed by a degenerate set of states at the same energy. As is a well known result ([58]), the degeneracies of the states converge to the values indicated in Table 4.2 as the number of electrons is increased, while for finite electron numbers some of the states are missing (because a reason analogous to that explained for the missing of bosonic modes). For 3 to 9 electrons the degeneracies, obtained from our diagonalization results, are summarized in Table 4.3 for later use. Clearly the counts converge to the even and odd sectors of the Table 4.2 for

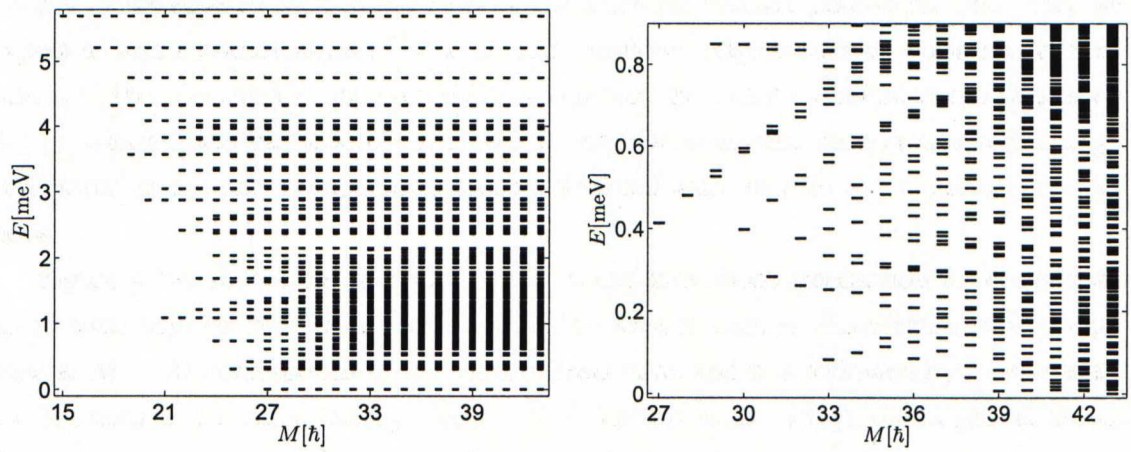

Figure 4.19: (a) The spectrum of the model three-body interaction (Equation 3.2.7), and (b) part of the low-energy spectrum in the presence of an additional repulsive potential at the center, both for 6 electrons.

even and odd electron numbers N, respectively.

To understand the low-energy spectrum, we introduce a gaussian quasihole trapping potential at the center of the droplet. As we break the degeneracy of the states, we see, which of them are related to quasihole excitations. The interesting part of the spectrum is shown in Figure 4.19b. As the angular momentum change corresponding to one quasihole is $\frac{N}{2}$, the interesting sequences of modes start from 30, 33, and 36. Starting from 30, the first low-energy states count as 1, 2, 4, 7, which indicates the change in the boundary conditions of the edge modes from periodic to anti-periodic caused by a half-flux quantum at the center (the last count is 7 instead of 8 due to missing states, as transition between even and odd sectors should not happen). At 33, the corresponding count starts 1, 1, which is consistent with the boundary conditions returning to periodic. However, more electrons should be included for a more reliable count. At 36, a similar dubious count 1, 2 indicates again anti-periodic boundary conditions. In the thermodynamic limit, the three cases correspond to quasiholes of charge $\frac{e}{4}$, $\frac{e}{2}$ and $\frac{3e}{4}$, respectively.

Table 4.2: The number of edge states of the Pfaffian state at angular momenta ΔM relative to the ground-state.

ΔM	0	1	2	3	4	5	6	7	8	b.c.	sector
	1	1	3	5	10	16	28	43	70	−	even
	1	2	4	7	13	21	35	55	86	−	odd
	1	2	4	8	14	24	40	64	100	+	both

Table 4.3: The number of edge modes and the LLL angular momentum of Moore-Read state for finite electron numbers.

ΔM	0	1	2	3	4	5	6	7	8	N	M
	1	2	3	4	6	7	9	11	13	3	5
	1	1	3	4	7	9	13	16	22	4	10
	1	2	4	6	10	14	20	27	36	5	18
	1	1	3	5	9	13	21	28	41	6	27
	1	2	4	7	12	18	28	40	57	7	39
	1	1	3	5	10	15	25	36	55	8	52
	1	2	4	7	13	20	32	48	71	9	68

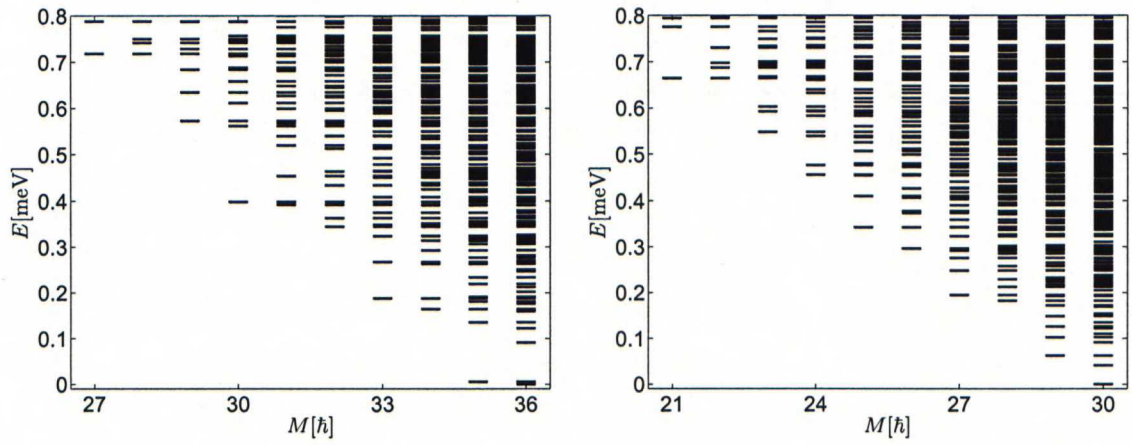

Figure 4.20: The spectrum of the Coulomb interaction of (a) the lowest and (b) the second lowest Landau level starting from the Moore-Read state angular momentum, $M = 27, 21$ on the two Landau levels, respectively. Six electrons in both.

Let us now consider the spectra evaluated with realistic interactions. In Figure 4.20, with the pure Coulomb interaction the edge modes starting from the Pfaffian state $M = 27$ (LLL) and 21 (SLL) are severely mixed with the bulk excitations on both of the two lowest Landau levels. Interestingly, on the LLL, there is a clear sequence of modes 1, 2, 4 starting from $M = 30$ corresponding to a half-vortex at the center and the change of the boundary conditions as above. The overlap of the LLL ground-state at $M = 30$ with the Pfaffian with half a flux vortex at the center is about 0.94. The wave function for the latter was obtained by diagonalizing the 3-body interaction with $M = 30$ and a tiny local repulsive potential that breaks the degeneracy and picks up the quasihole state. Optimal screening on the LLL or finite-thickness on the SLL can be used to reduce the mixing effects.

In the calculations of the previous subsection, the overlap with the Pfaffian state was at highest for 4 electrons on the SLL with screening $d_s \approx 0.8l$. The edge spectra corresponding to that screening for 4 and 5 electrons are shown in Figure 4.21. For 4 electrons, the angular momentum of the Pfaffian state is $M = 6$, and the corresponding first edge modes are counted to be 1, 1, 3, 5 and 9. In comparison with the Table 4.3, there are one and two states too many at $\Delta M = 3$ and 4 indicating a mixing to bulk excitations. For five electrons, the state corresponding to the Pfaffian (which is only defined for even electron numbers) has $M = 13$ ($M = 18 - 5$ on the SLL), and the corresponding count 1, 2, 4, 7 is consistent with the U(1)×Majorana edge theory for odd electron numbers, except for

one mixed-state at $\Delta M = 3$.

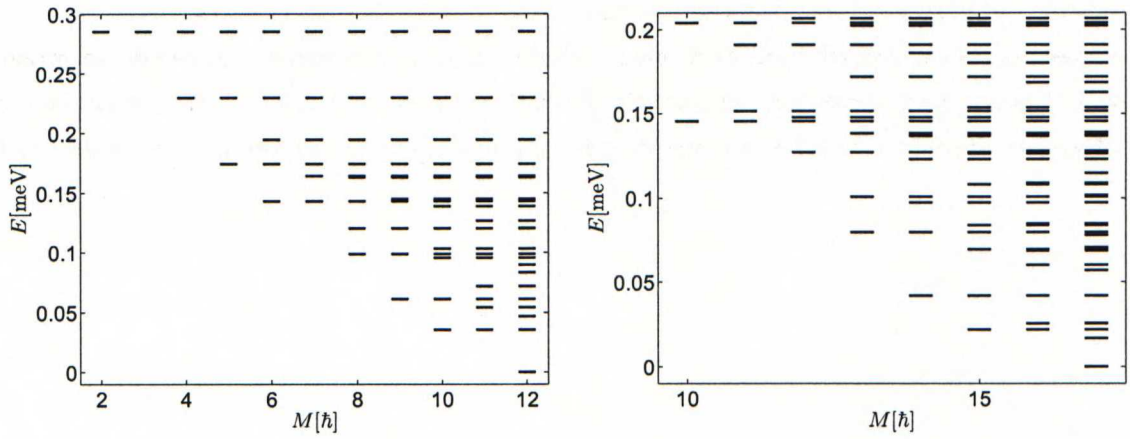

Figure 4.21: The spectrum of the SLL screened Coulomb interaction for (a) 4 and (b) 5 electrons with screening $d_s = 0.8l$.

4.3.3 Density fluctuations near charge of half a quantum vortex

In the previous spectral analysis, we referred to the charge $\frac{e}{4}$ quasihole realized in the Moore-Read quantum Hall state at the thermodynamic limit. In a finite system with a boundary, the charge fluctuations are strong and the quasihole charge may be obscured. Figure 4.22 shows the cumulative charge for a quasihole at the center of the droplet for the model interaction and Coulomb interaction on the lowest Landau levels. For the three-body interaction, the maximum of cumulative charge is below $0.35e$, and for the Coulomb interaction it is about $0.4e$ except for $N = 8$ where a double-peak structure of the density profile leads in this case to a large finite-size effect. The results qualitatively resemble those obtained for the Laughlin's quasiholes at $\nu = \frac{1}{3}$, and the cumulative charge is quantitatively lower approximately in the ratio $\frac{1}{4} : \frac{1}{3}$, which is also correct for the theoretical values of the charges in the Pfaffian and Laughlin description.

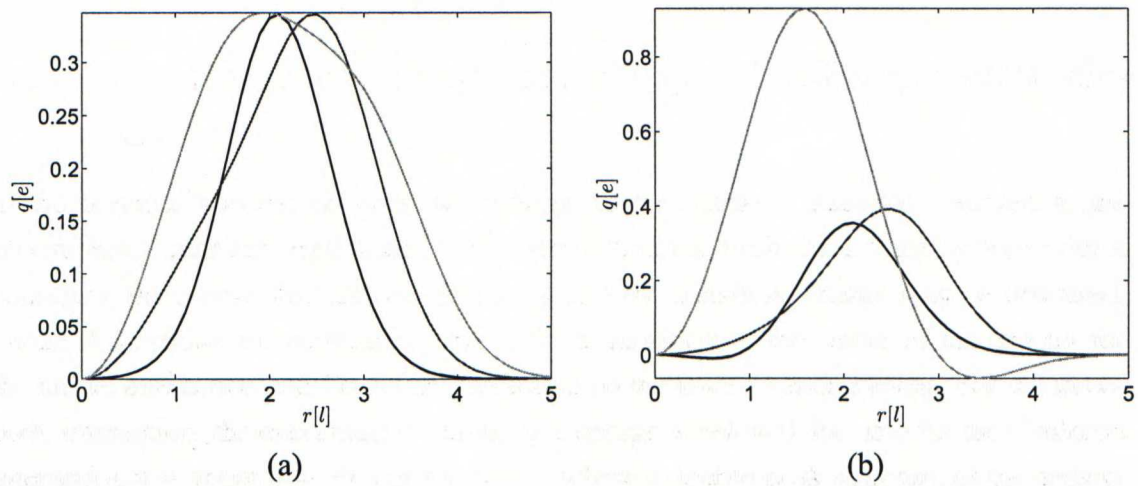

Figure 4.22: Cumulative quasihole charges at filling fraction $\frac{1}{2}$ for (a) the three-body interaction and (b) the Coulomb interaction for an elementary quasihole at the center with 4 (darkest), 6, and 8 (lightest) electrons.

Chapter 5

Discussion

We have investigated quantum Hall states in a quantum dot geometry at a high magnetic field when the Landau level projection, namely the assumption that the processes that do not conserve the Landau level index can be neglected, is applicable.

The ground-state phase diagram with effective Coulomb interactions corresponding to different Landau levels and sample details showed a rich structure of various phases. We have established the stability of phases corresponding to the Laughlin states and the Moore-Read state. Moreover, we have established a break-down of the Laughlin state in the form of an unbinding transition of flux and charge as the layer thickness is increased or too strong localization potential is introduced by investigating the overlaps and phase structure of the wave functions. The Laughlin wave function became exact, and thus strong flux-binding was achieved, for strongly screened interactions. Similarly, we have studied the phases corresponding to the Moore-Read state on the lowest and second lowest Landau level with realistic interactions and found that the overlap with the Moore-Read state significantly increases when the screening and thickness parameters are optimized to maximize the overlap.

We have further studied the charge fluctuations associated with quasihole excitations in the above phases. However, in a small system the finite-size effects are strong and the dependence of the quasihole charge on the position is evident. Still, the results fluctuate close to the correct charges, $\frac{e}{3}$ and $\frac{e}{4}$ for $\nu = \frac{1}{3}$ and $\nu = \frac{1}{2}$, respectively, in accordance with the theory. In addition, we have studied the low-energy excitation spectra and found patterns of energy states corresponding to the edge modes associated with the universality classes of Laughlin and Moore-Read states. These are a chiral boson mode for the

Lauhlin states and a chiral boson mode combined with a chiral Majorana fermion for the Moore-Read state. For realistic interactions, the edge modes mix with the bulk excitations, especially for large angular momenta relative to the ground-state, though the situation is improved in correlation with the overlap when the screening and layer-thickness are at optimal values. The change in the boundary conditions of the edge mode corresponding to creation of a half quantum vortex was also seen in the spectral analysis. Thus, the results of the long-range low-energy effective theory, albeit obscured, reach to the microscopic level.

Important omissions are the spin of the electron and Landau level mixing, which become more important on the higher Landau level systems, in which the magnetic field is not so strong. The analysis of the Pfaffian state in a quantum dot with dynamical spin and Landau level mixing is presented elsewhere [80]. If the Landau level mixing is treated perturbatively (although it may not be small in experiments), the result is a renormalization of the Coulomb interaction and a three-body interaction [81, 82], which ought to be weak for the perturbative analysis to make sense. The three-body interaction breaks the particle-hole symmetry in a half-filled Landau level, so that depending on the sign of the three-body term, either Pfaffian or the anti-Pfaffian is favored. However, there are also other inequivalent topological phases that can be responsible for the observed $\frac{5}{2}$-state, properties of which are listed in Ref. [83]. The actual experimental state can be distinguished by measuring the tunneling of quasiparticles at the edges of a quantum Hall bar, as different topological orders lead to different tunneling behaviour. The data of a recent experimental study [84] are most consistent with the anti-Pfaffian or an edge-reconstructed Pfaffian, the non-Abelian statistics of which are the same. An experimental observation of the non-Abelian statistics by interferometry experiments would be a serious milestone in the road towards an anyon quantum computer.

Bibliography

[1] A. Comtet, T. Jolicœur, S. Ouvry, and F. David, eds.,
Topological Aspects of Low Dimensional Systems - Les Houches, Session LXIX,
Springer, Berlin (2000).

[2] K. von Klitzing, G. Dorda, and M. Pepper,
New method for high-accuracy determination of the fine-structure constant based on quantized Hall resistance,
Phys. Rev. Lett. **45**, 494 (1980).

[3] D. C. Tsui, H. L. Stormer, and A. C. Gossard,
Two-dimensional magnetotransport in the extreme quantum limit,
Phys. Rev. Lett. **48**, 1559 (1982).

[4] A. Khare,
Fractional Statistics and Quantum Theory,
World Scientific, Singapore (1997).

[5] Y. Aharonov and D. Böhm,
Signifigance of electromagnetic potentials in the quantum theory,
Phys. Rev. **115**, 485 (1959).

[6] R. B. Laughlin,
Anomalous quantum Hall effect: An incompressible quantum fluid with fractionally charged excitations,
Phys. Rev. Lett. **50**, 1395 (1983).

[7] J. K. Jain,
Composite-fermion approach for the fractional quantum Hall effect,
Phys. Rev. Lett. **63**, 199 (1989).

[8] J. J. Quinn, A. Wójs, K. S. Yi, and J. J. Quinn,
Composite fermions in quantum Hall systems,
Int. School of Physics Enrico Fermi, Varenna (2003).

[9] Z. F. Ezawa,
Quantum Hall Effects - Field Theoretical Approach and Related Topics,
World Scientific, Singapore (2000).

[10] R. B. Laughlin,
Quantized Hall conductivity in two dimensions,
Phys. Rev. B **23**, 5632 (1981).

[11] B. I. Halperin,
Quantized Hall conductance, current-carrying edge states, and the existence of extended states in a two-dimensional disordered potential,
Phys. Rev. B **25**, 2185 (1982).

[12] D. J. Thouless, M. Kohmoto, M. P. Nighingale, and M. den Nijs,
Quantized Hall conductance in a two-dimensional periodic potential,
Phys. Rev. Lett **49**, 405 (1982).

[13] J. E. Avron and R. Seiler,
Quantization of the Hall conductance for general, multiparticle Schrödinger Hamiltonians,
Phys. Rev. Lett **54**, 259 (1985).

[14] F. E. Camino, Wei Zhou, and V. J. Goldman,
Realization of a Laughlin quasiparticle interferometer: observation of fractional statistics,
Phys. Rev. B **72**, 75342 (2005).

[15] F. E. Camino, Wei Zhou, and V. J. Goldman,
e/3 Laughlin quasiparticle primary-filling $\nu = 1/3$ *interferometer*,
Phys. Rev. Lett. **98**, 76805 (2007).

[16] D. Arovas, J. R. Schriffer, and F. Wilczek,
Fractional statistics and the quantum Hall effect,
Phys. Rev. Lett. **53**, 722 (1984).

[17] H. Kjønsberg and J. Myrheim,
Numerical study of the charge and statistics of Laughlin quasi-particles,
Int. J. Mod. Phys. A **14**, 537 (1999).

[18] H. Kjønsberg and J. M. Leinaas,
Charge and statistics of quantum Hall quasi-particles - a numerical study of mean values and fluctuations,
cond-mat/9901266v1 (1999).

[19] F. D. M. Haldane,
Fractional quantization of the Hall effect: A hierarchy of incompressible quantum fluid states,
Phys. Rev. Lett. **51**, 605 (1983).

[20] B. I. Halperin,
Statistics of quasiparticles and the hierarchy of fractional quantized Hall states,
Phys. Rev. Lett. **52**, 1583 (1984).

[21] E. Fradkin, C. Nayak, A. Tsvelik, F. Wilczek,
A Chern-Simons effective field theory for the Pfaffian quantum Hall state,
Nucl. Phys. B **546**, 711 (1997).

[22] N. Read and D. Green,
Paired states of fermions in two dimensions with breaking of parity and time-reversal symmetries and the fractional quantum Hall effect,
Phys. Rev. B **61**, 10267 (2000).

[23] G. Möller and S. H. Simon,
Paired composite-fermion wave functions,
Phys. Rev. B **77**, 75319 (2008).

[24] C. Nayak and F. Wilczek,
2n-quasihole states realize 2^{n-1} dimensional spinor braiding statistics in paired quantum Hall states,
Nucl. Phys. B **479**, 529 (1996).

[25] N. Read and G. Moore,
Fractional quantum Hall effect and nonabelian statistics,
Prog. Theor. Phys. Suppl. **107**, 157 (1992).

[26] S. Das Sarma, M. Freedman, C. Nayak, S. H. Simon, and A. Stern,
Non-Abelian anyons and topological quantum computation,
cond-mat/0707.1889v2 (2007).

[27] N. Read and E. H. Rezayi,
Beyon paired quantum Hall states: Parafermions and incompressible states in the first excited Landau level,
Phys. Rev. B **59**, 8084 (1999).

[28] E. H. Rezayi and N. Read,
Non-Abelian quantized Hall states if electrons at filling factors 12/5 and 13/5 in the first excited Landau level,
cond-mat/0608346v1 (2006).

[29] J. M. Leinaas and J. Myrheim,
On the theory of identical particles,
Il Nuovo Cimento **37**, 1 (1977).

[30] F. Wilczek, ed.,
Fractional Statistics and Anyon Superconductivity,
World Scientific, Singapore (1990).

[31] F. Wilczek,
Magnetic flux, angular momentum, and statistics,
Phys. Rev. Lett. **48**, 1144 (1982).

[32] F. Wilczek,
Quantum mechanics of fractional-spin particles,
Phys. Rev. Lett. **49**, 957 (1982).

[33] Y. S. Wu,
General theory for quantum statistics in two dimensions,
Phys. Rev. Lett. **52**, 2103 (1984).

[34] E. Artin,
Theory of braids,
Ann. of Math. **48**, 101 (1947).

[35] V. Gurarie and C. Nayak,
A plasma analogy and Berry matrices for non-Abelian quantum Hall states,
Nucl. Phys. B **506**, 685 (1997).

[36] E. Witten,
Quantum field theory and the Jones polynomial,
Comm. Math. Phys. **121**, 351 (1989).

[37] P. Di Francesco, P. Mathieu, and D. Sénéchal,
Conformal Field Theory,
Springer, New York (1999).

[38] E. Brézin and J. Zinn-Justin, eds.,
Fields, Strings and Critical Phenomena - Les Houches, Session XLIX,
Elsevier, North-Holland (1989).

[39] R. Hanson, L. P. Kouwenhoven, J. R. Petta, S. Tarucha, and L. M. K. Vandersypen,
Spins in few-electron quantum dots,
Rev. Mod. Phys. **79**, 1217 (2007).

[40] R. Shankar,
Chaotic quantum dots with strongly correlated electrons,
Rev. Mod. Phys. **80**, 379 (2008).

[41] S. M. Reimann and M. Manninen,
Electronic structure of quantum dots,
Rev. Mod. Phys. **74**, 1283 (2002).

[42] S. M. Girvin and A. H. MacDonald,
Off-diagonal long-range order, oblique confinement, and the fractional quantum Hall effect,
Phys. Rev. Lett. **58**, 1252 (1987).

[43] S. C. Zhang, T. H. Hansson, and S. Kivelson,
Effective field theory for the fractional quantum Hall effect,
Phys. Rev. Lett **62**, 82 (1989).

[44] S. C. Zhang,
The Chern-Simons-Landau-Ginzburg theory of the fractional quantum Hall effect,
Int. J. Mod. Phys. B **6**, 25 (1992).

[45] B. Blok and X. G. Wen,
Effective theories of the fractional quantum Hall effect: hierarchy construction,
Phys. Rev. B **42**, 8145 (1990).

[46] B. Blok and X. G. Wen,
Effective theories of the fractional quantum Hall effect at generic filling fractions,
Phys. Rev. B **42**, 8133 (1990).

[47] A. Lopez and E. Fradkin,
Fractional quantum Hall effect and Chern-Simons gauge theories,
Phys. Rev. B **44**, 4821 (1991).

[48] A. Lopez and E. Fradkin,
Fermion Chern-Simons theory of hierarchical fractional quantum Hall states,
Phys. Rev. B **69**, 155322 (2004).

[49] X. G. Wen,
Topological orders and edge excitations in FQH states,
Adv. Phys. **44**, 405 (1995).

[50] X. G. Wen,
Theory of the edge states in fractional quantum Hall effects,
Int. J. Mod. Phys. B **6**, 1711 (1992).

[51] M. Levin and X. G. Wen,
Detecting topological order in a ground state wave function,
Phys. Rev. Lett. **96**, 110405 (2006).

[52] X. G. Wen, Y. S. Wu, Y. Hatsugai,
Chiral operator algebra and edge excitations of a fractional quantum Hall droplet,
Nucl. Phys. B **422**, 476 (1994).

[53] S. Siljamäki,
Quantum Monte Carlo calculations of a few-electron quantum dots in high magnetic field,
M. Sc. thesis, Helsinki University of Technology (1999).

[54] M. E. Peskin and D. V. Schroeder,
An Introduction to Quantum Field Theory,
Westview, Colorado (1995).

[55] V. F. R. Jones,
A polynomial invariant for knots via von Neumann algebras,
Bull. Amer. Math. Soc **12**, 103 (1985).

[56] E. Witten,
Global aspects of current algebra,
Nucl. Phys. B **223**, 422 (1983).

[57] J.Wess and B. Zumino.
Consequences of anomalous Ward identities,
Phys. Lett. B **37**, 95 (1971).

[58] X. G. Wen,
Topological order and edge structure of $\nu = \frac{1}{2}$ *quantum Hall state*,
Phys. Rev. Lett. **70**, 355 (1993).

[59] N. W. Ashcroft and N. D. Mermin,
Solid State Physics,
Holt, Rinehart and Winston, New York (1976).

[60] M. J. Manfra, R. de Picciotto, Z. Jiang, S. H. Simon, L. N. Pfeiffer, K. W. West, and A. M. Sergent,
Impact of spin-orbit coupling on quantum Hall nematic phases,
Phys. Rev. Lett. **98**, 206804 (2007).

[61] J. Suorsa,
Phase vortices and many-body states in the lowest Landau level,
M. Sc. thesis, Helsinki University of Technology (2006).

[62] E. V. Tsiper,
Analytic Coulomb matrix elements in the lowest Landau level in disk geometry,
J. Math. Phys. **43**, 1664 (2002).

[63] R. E. Prange and S. M. Girvin, eds.,
The Quantum Hall Effect,
Springer, New York (1990).

[64] S. H. Simon, E. H. Rezayi, and N. R. Cooper,
Pseudopotentials for multiparticle interactions in the quantum Hall regime,
Phys. Rev. B **75**, 195306 (2007).

[65] X. Wan, Z. X. Hu, E. H. Rezayi, and K. Yang,
Fractional quantum Hall effect at $\nu = 5/2$*: ground states, non-Abelian quasiholes, and edge modes in a microscopic model*,
Phys. Rev. B **77**, 165316 (2008).

[66] M. Greiter, X. G. Wen, and F. Wilczek,
On paired Hall states,
Nucl. Phys. B **374**, 567 (1992).

[67] J. Nissinen,
Conformal field theory and numeric for fractional quantum Hall systems,
M. Sc. thesis, Helsinki University of Technology (2008).

[68] J. M. Thijssen,
Computational Physics,
Cambridge University Press, Cambridge (1999).

[69] D. Chruściński and A. Jamiołkowski,
Geometric Phases in Classical and Quantum Mechanics,
Birkhäuser, Boston (2004).

[70] M. V. Berry,
Quantal phase factors accompanying adiabatic changes,
Proc. R. Lond. **A392**, 45 (1984).

[71] B. Simon,
Holonomy, the quantum adiabatic theorem, and Berry's phase,
Phys. Rev. Lett. **51**, 2167 (1983).

[72] F. Wilczek and A. Zee,
Appearance of gauge structure in simple dynamical systems,
Phys. Rev. Lett. **52**, 2111 (1984).

[73] A. Shapere and F. Wilczek, eds.,
Geometric Phases in Physics,
World Scientific, Singapore (1989).

[74] Y. Tserkovnyak and S. H. Simon,
Monte-Carlo evaluation of non-Abelian statistics,
Phys. Rev. Lett. **90**, 16802 (2003).

[75] C. Moler and C. Van Loan,
Nineteen dubious ways to compute the exponential of a matrix, twenty-five years later,
SIAM Rev. **45-1**, 3 (2003).

[76] W. Y. Ruan, Y. Y. Liu, C. G. Bao, and Z. Q. Zhang,
Origin of magic angular momenta in few-electron quantum dots,
Phys. Rev. B **51**, 7942 (1995).

[77] T. Seki, Y. Kuramoto, and T. Nishino,
Origin of magic angular momentum in a quantum dot under strong magnetic field,
J. Phys. Soc. Jpn. **65**, 3945 (1996).

[78] J. K. Jain and T. Kawamura,
Composite fermions in quantum dots,
Europhys. Lett. **29**, 321 (1995).

[79] G. S. Jeon, C. C. Chang, J. K. Jain,
Semiconductor quantum dots in high magnetic fields: The composite-fermion view,
Eur. Phys. J. **55**, 271 (2007).

[80] H. Saarikoski, E. Tölö, A. Harju, and E. Räsänen,
Fragmentation of the $\nu = \frac{5}{2}$ quantum Hall state in quantum dots,
to be published, (2008).

[81] S. S. Lee, S. Ryu, C. Nayak, and M. P. A. Fisher,
Particle-hole symmetry and the $\nu = \frac{5}{2}$ quantum Hall state,
Phys. Rev. Lett. **99**, 236807 (2007).

[82] S. H. Simon,
Effect of Landau level mixing on braiding statistics,
Phys. Rev. Lett. **100**, 116803 (2008).

[83] B. J. Overbosch and X. G. Wen,
Phase transition on the edge of the $\nu = \frac{5}{2}$ Pfaffian and anti-Pfaffian quantum Hall state,
cond-mat/0804.2087 (2008).

[84] I. P. Radu, J. B. Miller, C. M. Marcus, M. A. Kastner, L. N. Pfeiffer, and K. W. West,
Quasiparticle properties from tunneling in the $\nu = 5/2$ fractional quantum Hall state,
Science **320**, 899 (2008).